$(p,p'\pi^+)$ reaction at energies below 1 GeV

B. K. Jain
Nuclear Physics Division, Bhabha Atomic Research Centre, Bombay 400 085, India

J. T. Londergan and G. E. Walker
Department of Physics and Nuclear Theory Center, Indiana University, Bloomington, Indiana 47405
(Received 31 August 1987)

The features of the $(N,N'\pi)$ reaction are examined at intermediate energies, i.e., for 300–800 MeV incident nucleon energies, when the continuum nucleon and pion are observed in coincidence. In comparison with the (N,π) reaction, which has been studied in considerable detail both theoretically and experimentally, there are some advantages in analyzing the $(N,N'\pi)$ reaction. Both reactions can deliver large momentum transfer to the nucleus; however, the $(N,N'\pi)$ reaction can also occur for relatively small momentum transfer (e.g., $q \approx 200$ MeV/c). Thus this reaction can be studied in regions where nuclear single-particle wave functions and transition densities are large and well known. In this paper we consider one particular reaction: the exclusive $(p,p'\pi^+)$ reaction. For this process we focus on the amplitudes which are dominated by a $\Delta(1232)$ resonance in intermediate states. A nonrelativistic formalism for the reaction amplitudes is derived and examined in detail. The theoretical cross sections are shown to be quite sensitive to the pion self-energy, and relatively insensitive to the isobar self-energy in the medium. Furthermore, the calculations suggest that certain amplitudes may dominate the cross sections in different kinematic regions. The differences between relativistic and nonrelativistic approximations for the pion self-energy are examined. Because of the exploratory nature of this investigation, simple forms are used for the bound-state wave functions and transition densities, and the continuum particles are approximated by plane waves; the effects of distorted waves are estimated.

I. INTRODUCTION

For several years, the study of pion production in nucleon-induced reactions has been the subject of both theoretical and experimental interest. There is now a considerable body of experimental data on pion production, for both π^+ and π^- reactions.[1–3] It includes both exclusive and inclusive spectra. From the theoretical and experimental studies of these processes[4–8] some progress in understanding has been achieved, though theoretical investigations of (N,π) reactions have encountered difficulties in reproducing the quantitative features of the data.

A characteristic feature of the (p,π) reaction is that it is a high momentum transfer process. The process thus samples nuclear wave functions in a region where they are small and not well known from other experiments. This is a desirable feature if one is trying to identify the high-momentum components of nuclear wave functions; however, such reactions have the intrinsic difficulty that more than one target nucleon may participate actively in the reaction, and the resulting cross sections can be quite sensitive to a number of different processes.

In contrast, in the $(N,N'\pi)$ reaction where both the outgoing nucleon and pion are observed in coincidence, the momentum transfer can be relatively small. For example, for a proton incident energy of 450 MeV and outgoing proton energy greater than 100 MeV, for forward outgoing nucleons, the momentum transfer to the nucleus does not vary greatly: the minimum momentum transfer is between 200–250 MeV/c for incident protons between 400 and 700 MeV. Thus, this reaction can reach lower momentum transfers than are possible with (p,π), while for other kinetic configurations it can also probe very high momentum transfers. It may be possible to fit the $(N,N'\pi)$ reaction in a regime where the momentum transfer is small, and then extrapolate into a regime where the theoretical situation is much less certain. Experimentally, the situation for the $(N,N'\pi)$ reaction is somewhat more complicated than for the (N,π) reaction, as it requires observation of two energetic final particles in coincidence; however, with current medium-energy machines this should not be too difficult. For example, in the Indiana University Cyclotron Facility (IUCF) cooler now under construction, it would be possible to observe the outgoing nucleon in coincidence with the pion.[9]

We assume that the $(N,N'\pi)$ reaction proceeds through a quasifree $NN \rightarrow NN\pi$ amplitude, modified in the nuclear environment. Since the final nucleon is unbound, this assumption about the reaction mechanism for $A(N,N'\pi)B$ should be more valid than for the (p,π) reaction. Furthermore, in pp collisions at the National Laboratory for High Energy Physics (KEK), Shimizu *et al.*[10,11] showed that, for proton lab energies from 360–1300 MeV, the $pp \rightarrow NN\pi$ process proceeds dominantly through an intermediate real Δ isobar.[10] Therefore, we assume that the $A(N,N'\pi)B$ reaction also proceeds through a Δ in the intermediate state. This may particularly be true for the $(p,p'\pi^+)$ reaction, as 80% of the free $pp \rightarrow np\pi^+$ cross section has been found to

proceed through $pp \rightarrow n\Delta^{++}$ for proton incident energies from 550 to 1300 MeV.[11] This paper thus focuses on the (p,p'π^+) reaction, leading to exclusive final nuclear states. It is assumed that such a process is dominated by the production, propagation, and decay of a Δ isobar.

Previous theoretical calculations of (N,N'π) reactions have been carried out for elastic (p,nπ^+) reactions on isoscalar closed-shell targets. The motivation for these studies was very different from ours. The aim of these earlier calculations was to minimize the role of the isobar in order to examine the dependence of theoretical calculations, on the form of the NNπ vertex, or on the nonrelativistic (NR) reduction of the relativistic vertex. These calculations were carried out in the "one-nucleon-mechanism" framework for pion production in nucleon-induced reactions. Sherif *et al.*[12] examined the dependence of the cross sections for ^{4}He(p,nπ^+)^{4}He on the form of the nonrelativistic reduction of the NNπ vertex; Greben and Woloshyn[13] have compared results for the same reaction using pseudoscalar (PS) or pseudovector (PV) NNπ couplings, and they have compared various nonrelativistic reductions with the relativistic results. These authors find very large differences depending on the type of vertex and the form of the nonrelativistic reduction.

In our calculation, we have chosen a reaction which should emphasize the role of the intermediate isobar, and we work in the "two-nucleon" framework, where the pion is created through the NN$\rightarrow$NNπ reaction in the nuclear medium. Our amplitudes are very similar in principle with those of the isobar-hole model;[15] such amplitudes have been widely used in pion-nucleus elastic and inelastic reactions in this energy region. Therefore, it is unlikely that the uncertainties in our amplitudes should be nearly as large as those suggested in Refs. 12 and 13. A recent relativistic distorted-wave impulse approximation (DWIA) calculation of the elastic (p,nπ^+) reaction has been carried out on ^{16}O by Cooper *et al.*;[14] they use relativistic distorted waves for the nucleons and pion, and a PV NNπ vertex. These authors find roughly a factor of 2 difference between their results, using a PS or PV NNπ vertex.

In Sec. II the particular amplitudes for the (p,p'π^+) reaction are presented in detail. As the aim is to examine the features of this reaction, we are interested in simple estimates of the relative size of the various reaction amplitudes, and in order-of-magnitude estimates of medium effects on intermediate mesons and isobars. Therefore, the first calculations are done with simple forms for the nuclear wave functions and transition densities, and with very simple approximations for the nucleon and pion wave functions. Due to these simplifying assumptions, the results should be considered exploratory. These assumptions will be removed in a subsequent calculation of this process. With these approximations, all reaction amplitudes can either be calculated analytically, or they can be written in terms of simple one-dimensional integrals. The resulting amplitudes and integrals are listed in Appendix A.

In Sec. III, the results of the calculations are presented and discussed. For the (p,p'π^+) exclusive reaction, the initial results are sensitive to several of the amplitudes. However, if the pion angle is fixed and the outgoing proton energy is varied, it appears possible to separate the different amplitudes. In Secs. III B–D the medium modifications to the cross sections are discussed. In Sec. III B, we discuss medium effects on the virtual meson. Such corrections lead to a considerable enhancement of the theoretical cross sections. In addition, one amplitude [the "projectile excitation" amplitude of Fig. 1(a)] tends to dominate the calculated cross sections when medium effects are included. Detailed equations for pion medium corrections are presented in Appendix B. In Appendix C, an alternative relativistic formalism is derived for the pion medium corrections. Results are derived for this case and compared with the NR results derived previously.

In Sec. III C, we discuss the dependence of the cross sections on the modification of the Δ in the medium. These modifications include the effects of the medium on the position and width of the isobar, through Pauli blocking and a complex spreading potential. The estimates of these quantities are based on quantitative calculations of the scattering and propagation of isobars in medium-energy reactions. It is shown that the medium effects on the intermediate isobars are considerably smaller than the medium effects estimated for the virtual mesons.

Section III concludes with a discussion of the effects of proton and pion distortions on the theoretical cross sections. We expect the major effects to be absorptive. An estimate is made for the absorption of the protons and the pion. It is found that these effects result in a decrease in the cross sections by a factor of 10–50, relative to the plane-wave calculations. In Sec. IV, the conclusions and further outlook for the (p,p'π^+) reaction are presented.

II. QUALITATIVE FEATURES OF THE (N,N'π) REACTION

The (p,p'π) reaction contains an outgoing proton, a pion and the recoil nucleus in the final state. Consequently, the final state of the system constitutes an intrinsic three-body problem. It therefore requires the treatment of the interactions of the initial and final-state protons with the nucleus, the final pion with the nucleus, and the mutual interaction between the final proton and pion. For this process, incident proton kinetic energies T_p from 300–800 MeV will be studied. At intermediate energies the most important term, which dominates the π^+p interaction, is the resonant interaction between the pion and the nucleon, producing the Δ (1232).

This work will consider those processes which involve explicit creation and propagation of the Δ, and its decay to a nucleon and a pion. In a subsequent work, the contribution of nonresonant amplitudes to this reaction will be investigated. The effects of the nuclear medium on the intermediate meson and isobar will be estimated. The first results will be presented in a plane-wave (PW) approximation for the continuum protons and pion. For most of the energies considered, the main effects of final-

state interactions will be absorptive. In a later section we estimate in an eikonal formalism the attenuation due to absorption of the initial and final particles. This exploratory work will determine the order of magnitude of the cross sections to be expected for this reaction, it will provide estimates of the medium effects on the meson and isobar, and it will discuss how energy and angular spectra can be used to gain information on the nuclear transition densities and the reaction amplitudes, respectively.

The particular reaction amplitudes which are studied in this paper are shown in Fig. 1. The incident proton is denoted by its momentum $\mathbf{k}$, the final proton by $\mathbf{k}'$. The wavy line preceding the formation of the Δ represents a meson, e.g., π, ρ or a heavy meson. Figures 1(b)–(d) are obtained from Fig. 1(a) by interchanging either the initial or final nucleons. The amplitudes shown in Fig. 1 are just those which have been calculated for the (p,π) reaction previously.[5,7] However, there are several differences between the two reactions. The first, as mentioned previously, is the momentum transfer to the nucleus. In the (N,N'π) reaction, the lowest momentum transfer is about

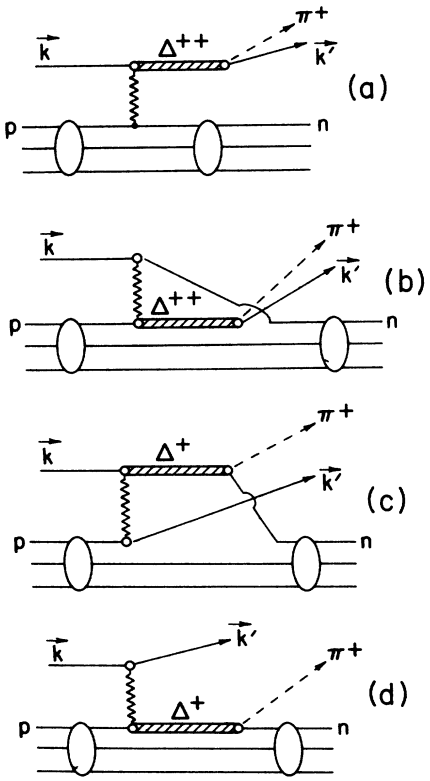

FIG. 1. Amplitudes considered for the (p,p'π^+) reaction. (a) "Projectile excitation" amplitude, incident proton with momentum $\mathbf{k}$ interacts with target proton (wavy line), exciting proton to a Δ^{++} isobar, which then decays to proton with momentum $\mathbf{k}'$ and π^+; (b) "target excitation" amplitude, target proton is excited to isobar. This amplitude is identical to (a) except that projectile and target protons in the initial state are interchanged; (c) projectile is excited to a Δ^+ isobar. This amplitude is similar to (a) except that the final-state neutron and proton are interchanged; (d) target nucleon is excited to a Δ^+, which decays to pion plus neutron. This amplitude is identical with (c) if the projectile and target protons in the initial state are interchanged.

1 fm^{-1}. This is much smaller than the corresponding value for the (N,π) reaction, and it is in a region where the nuclear wave functions and transition densities are large and are well known from other experiments.

We can see by inspection that the four amplitudes of Fig. 1 have quite different behavior for the (N,N'π) reaction. One way to see this is to examine the energy carried by the virtual meson and by the isobar in the four amplitudes of Fig. 1. In Fig. 1(a), the energy of the intermediate meson is given by the difference between the initial and final binding energies. The present work focuses on the excitation of low-lying nuclear states, for which this energy is quite small, and can be approximated by zero. The energy of the isobar in this amplitude is given by T_p+M_p, where T_p is the kinetic energy of the incident nucleon. This is a large energy, and it is independent of the kinematics of the final particles. In Fig. 1(b), the energy of the intermediate meson is T_p; the energy of the isobar is T_p+M_p, the same as in Fig. 1(a).

In Fig. 1(c), the energy of the intermediate meson is $T_{p'}$, the kinetic energy of the final proton. The energy of the isobar is $E_\pi+M_p$, where E_π is the total energy of the final pion. This energy is considerably smaller than the energy of the isobar corresponding to the amplitudes of Figs. 1(a) and (b); also, both the meson and isobar energies vary as we change the kinematics of the outgoing proton and pion. In Fig. 1(d), the energy of the intermediate meson is $T_p-T_{p'}$; the energy of the isobar is $E_\pi+M_p$, the same as for Fig. 1(c).

In the four amplitudes of Fig. 1, there is a tremendous variation in the energy of the virtual meson, from zero to the incident kinetic energy. As a consequence, the behavior of the four amplitudes could be quite different, and this might be exploited to separate the various amplitudes by varying the final-state kinematics. In the language of Oset *et al.*,[16,17] the amplitude of Fig. 1(a) represents the "acoustic mode" for pions, i.e., the regime where the energy of the pion is roughly zero and the momentum is of the order 1–3 fm^{-1}. Of the remaining amplitudes, Fig. 1(b) represents the "isobar mode," i.e., where the typical intermediate pion carries much of the energy necessary to excite the $\Delta(1232)$ resonance. Depending upon the final-state kinematics, Figs. 1(c) and (d) may also be in this region. The different amplitudes thus allow us to explore very different regions of the virtual meson propagator. However, estimating the self-energy contributions requires that one know the medium effects over a very wide range of energy and momenta.

In this work the angle of the outgoing proton is fixed at 10° relative to the incident proton direction. The peak cross sections are then found to occur for forward pions. These pion angles correspond to the minimum possible nuclear momentum transfer, about 200–250 MeV/c; this is roughly independent of incident proton energy from 300–800 MeV. The most important amplitudes for the (p,p'π^+) reaction in this kinematic region are the amplitudes of Figs. 1(a) and (d).

The various amplitudes can also be separated by spin and isospin considerations. For example, most previous theoretical calculations have been done for elastic scattering on a $T=0$ target. In this case, it is straightforward to

show that Figs. 1(a) and (b) give no contribution. We will discuss this in more detail in Sec. IV.

A. Formalism

The relativistic interaction Lagrangian for the coupling of a meson to a nucleon or a $\Delta(1232)$ isobar is given by

$$\mathcal{L}_{\rm int}=\frac{f_\pi}{m_\pi}\bar{\Psi}_N\gamma^\nu\gamma^5\tau\Psi_N\partial_\nu\cdot\Phi+\frac{f_\Delta}{m_\pi}(\bar{\Psi}^\nu_\Delta\mathbf{T}\Psi_N\partial_\nu\cdot\Phi+\text{H.c.}) . \tag{1}$$

For most of this paper, however, we will use the nonrelativistic reduction of this Lagrangian, i.e.,

$$\mathcal{L}_{\rm NR}=\frac{f_\pi}{m_\pi}\bar{\chi}_N\sigma\cdot\mathbf{q}\tau\chi_N\cdot\Phi+\frac{f_\Delta}{m_\pi}\bar{\chi}_\Delta\mathbf{S}\cdot\mathbf{q}\mathbf{T}\chi_N\cdot\Phi . \tag{2}$$

In Eq. (1), Ψ_N represent the nucleon Dirac four-component spinors and Ψ^ν_Δ represents the Δ spinor with covariant index ν. In Eq. (2), **T** and **S** are the isospin and spin transition matrices from $J=\frac{1}{2}$ to $\frac{3}{2}$, analogous to τ and σ, respectively, and **q** is the pion momentum. In these interactions, the coupling constants have the form of a "bare" coupling times a form factor, $f=f[F(q)]^{1/2}$, where the form factor $F(q)$ is assumed to be of monopole form

$$F(q)=\left[\frac{\Lambda^2-m_\pi^2}{\Lambda^2-\omega^2+q^2}\right]^2 . \tag{3}$$

In Eq. (3), the cutoff Λ is taken to be 1.2 GeV. We use the same cutoff for both NNπ and N$\Delta\pi$. This is similar to, for example, the latest Bonn NN potential.[18] The "bare" coupling constants are taken as $f_\pi^2/4\pi=0.08$ and $f_\Delta^2/4\pi=0.37$. The ΔNπ coupling constant reproduces the experimental Δ decay width (115 MeV) at resonance.[16,19] For the remainder of this paper, when $f(q)$ is used for a form factor, it includes the form factor F; when written as f, it represents the "bare" coupling constant.

The couplings outlined here are only those of a pion to nucleons and isobars. We could also include couplings of ρ mesons or other heavy mesons. However, for such contributions the contributions of the direct and exchange terms tend to cancel almost completely. This will be discussed in more detail in Sec. III C, where it will be shown that short-ranged contributions are extremely important in estimating pion self-energy contributions, but that the direct couplings of ρ or other heavy mesons should be quite small.

The amplitudes for the (p,p'π^+) reaction proceeding via an intermediate Δ state give rise to four terms, shown diagrammatically in Figs. 1(a)–(d). Note that diagrams of the form of Fig. 1(a) are included, but the "crossed" diagrams, of the type shown in Fig. 2, are not considered. The crossed diagrams should be considerably smaller than the "direct" diagrams; estimates of the size of the crossed diagrams in (p,π) reactions suggests that they are of the order of 10% or smaller relative to the direct diagrams.[20] In addition, the isospin coupling coefficients for the (p,p'π^+) reaction suppress the contribution of Fig. 2 by a factor of 3 relative to the contribution from Fig. 1(a).

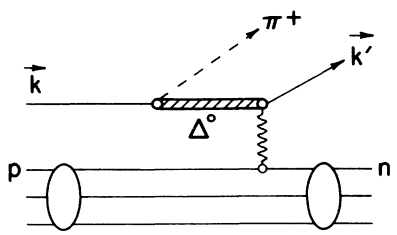

FIG. 2. The analog of Fig. 1(a) if the pion is emitted at the first isobar vertex. In this "crossed' graph the intermediate isobar is a Δ^0.

As will be shown later, the amplitude of Fig. 1(a) gives the dominant contribution to the calculated cross sections; therefore, terms such as those in Fig. 2 have been neglected in this work.

The amplitude of Fig. 1(a) corresponds to emission of a virtual meson from a target nucleon, excitation of the incident proton to a $\Delta(1232)$, with subsequent decay to a continuum proton and pion; thus, we refer to this amplitude as the "projectile excitation" term. For "amplitude A" [referring to the diagram of Fig. 1(a)], the expression has the form

$$T_A=\sqrt{2}\rho^{\sigma\tau}_{fi}(\mathbf{q}_A)\frac{ff_\Delta^2}{m_\pi^3}F(q_A)\frac{\langle k'|\mathbf{S}^\dagger\cdot\mathbf{k}_\pi\mathbf{S}\cdot\mathbf{q}_A|k\rangle}{D_\Delta(q_A^\Delta,\omega_A^\Delta)D_\pi(q_A,\omega_A)} , \tag{4}$$

where

$$\begin{aligned}&\mathbf{q}_A=\mathbf{k}_\pi+\mathbf{k}'-\mathbf{k},\quad \omega_A=\epsilon_f-\epsilon_i\approx 0\\ &\mathbf{q}_A^\Delta=\mathbf{k}_\pi+\mathbf{k}',\quad \omega_A^\Delta=E'+E_\pi .\end{aligned} \tag{5}$$

The subscript A refers to the amplitude in question.

In Eq. (4), D_Δ represents the propagator for the intermediate Δ, and D_π is the propagator for the meson exchanged between the projectile and target nucleons (for the time being, we will take this as a pion). The incident and final proton states are denoted by k and k', and the initial bound proton and final bound neutron are denoted by i and f, respectively. As mentioned in the last section, the fourth component of the virtual meson momentum, ω_A, is given by the difference in binding energy of the initial proton and the final neutron. In comparison with the three-momentum q_A,ω_A can be set to zero.

The spin-isospin transition matrix $\rho^{\sigma\tau}$ in Eq. (4) is given by

$$\rho^{\sigma\tau}_{fi}(\mathbf{q})=\left\langle f\left|\sum_j\sigma_j\cdot\mathbf{q}\tau_j^-\right|i\right\rangle , \tag{6}$$

where the initial and final nuclear states are denoted by i and f, respectively, and the sum is over all target nucleons. For this paper we will consider cases where the final state is a single neutron particle-proton hole state relative to the initial state, and we assume that the core is inert, in which case Eq. (6) can be written

$$\rho^{\sigma\tau}_{fi}(\mathbf{q})=\langle\phi_{n,f}|\sigma\cdot\mathbf{q}|\phi_{p,i}\rangle . \tag{7}$$

In Eq. (7), only a single "active" nucleon contributes to

the transition density.

In this paper, the aim is to explore the general features of the (p,p'π^+) reaction. Therefore, we have used simple Gaussian forms for the single-particle transition densities and wave functions,

$$\phi(p)=\left[\frac{4\pi}{p_0^2}\right]^{3/4}\exp(-p^2/2p_0^2)\ , \tag{8}$$

$$\rho(p)=\exp(-p^2/4p_0^2)\ . \tag{9}$$

The model wave functions thus depend upon a single momentum scale, p_0. This parameter has been fixed by requiring that it reproduce the same mean squared single-particle momentum seen in electron scattering data. In terms of the Fermi momentum, p_0 then obeys the relation

$$p_0^2=\tfrac{2}{3}\langle p^2\rangle=\tfrac{2}{5}k_F^2\ . \tag{10}$$

These nuclear wave functions are oversimplified and lack the dependence on orbital and spin degrees of freedom. They reproduce single-particle momentum distributions for the nucleus as a whole, rather than being typical of a particular shell. Also, they fall off too fast for large momentum. Therefore, our resulting cross sections will decrease too rapidly away from the peak cross sections. These wave functions are also structureless; they have no minima, for example. As a result, effects due to minima in the nuclear wave functions will not be present in our calculations. However, we have deliberately chosen featureless wave functions for this initial survey, as it is well known that PW approximations can overestimate the effects of structure (and, particularly minima) in single-particle wave functions: for example, a PW approximation involving a bound-state wave function with a zero will frequently produce a deep minimum in a cross section, whereas the minimum may be completely "filled in" when distortions are included.

The effects of distortions will be estimated in Sec. III D. For the protons, distortion effects should mainly involve absorption; this will be the case except when the outgoing proton kinetic energy is very small, in which case dispersive effects should become important. Overall effects of proton distortions should be reasonably small. For example, Cooper *et al.*[14] calculate such effects and find that the proton and (in their case) neutron distortions each produce roughly a factor of 2 decrease in the cross sections. For the pion, the effects of final-state interactions will be more drastic. Again, the pion-nucleus distortion effects will be primarily absorptive, and mainly due to "nucleon knock-out" by the final pion, and "real absorption" of the pion. These distortion effects should have two qualitative effects on the calculated cross sections: first, they should produce a rather large decrease in the cross sections. By comparing plane-wave and distorted-wave calculations of (p,π) reactions, the final-state interactions will be seen to decrease our cross sections by about an order of magnitude relative to the PW results. Secondly, the strong absorption of the outgoing pion will make these reactions surface peaked: the pion is preferentially produced at the surface of the nucleus (otherwise, it gets absorbed on the way out), where the nuclear density is only a fraction of the central density. Detailed estimates of these effects will be presented in Sec. III D.

The pion and Δ propagators are given by

$$D_\pi(\mathbf{q},\omega)=[\omega^2-\mathbf{q}^2-m_\pi^2-\Pi(\mathbf{q},\omega)+i\epsilon]^{-1}\ , \tag{11}$$

for the pion, where Π is the self-energy of the pion with momentum q and energy ω; similarly, the Δ propagator is given by

$$D_\Delta(\mathbf{q},\omega)=[\omega-T_\Delta-M_\Delta-\mathcal{V}_\Delta(q,\omega)+i\Gamma/2+i\epsilon]^{-1}\ , \tag{12}$$

where $\mathcal{V}$ represents the real part of the nuclear potential for a Δ with energy ω and momentum q, T_Δ is the kinetic energy and Γ the width of the isobar. In this form the (nonlocal) isobar-nucleus interaction has been approximated by a local effective potential.

The second amplitude considered in this model corresponds to emission of a meson by the projectile proton, as shown in Fig. 1(b). This meson excites a target nucleon to a Δ, which then decays to the final continuum proton and pion. We refer to this amplitude as the "target excitation" term (or "amplitude B"). This amplitude has the form

$$T_B=\sqrt{2}\frac{f_\pi f_\Delta^2}{m_\pi^3}\int\frac{d\mathbf{q}}{(2\pi)^3}\frac{F(q)\phi_f^\dagger(\mathbf{k}-\mathbf{q})\phi_i(\mathbf{k}'+\mathbf{k}_\pi-\mathbf{q})}{D_\Delta(q_B^\Delta,\omega_B^\Delta)D_\pi(q,\omega_B)}$$
$$\times\langle f\,|\,\boldsymbol{\sigma}\cdot\mathbf{q}\,|\,k\rangle\langle k'\,|\,\mathbf{S}^\dagger\cdot\mathbf{k}_\pi\mathbf{S}\cdot\mathbf{q}\,|\,i\rangle\ , \tag{13}$$

where

$$\begin{aligned}&\omega_B=T_p+\epsilon_f\approx T_p\ ,\\ &\mathbf{q}_B^\Delta=\mathbf{k}'+\mathbf{k}_\pi=\mathbf{q}_A^\Delta\ ,\\ &\omega_B^\Delta=E'+E_\pi=\omega_A^\Delta\ .\end{aligned} \tag{14}$$

This amplitude is proportional to the product of two single-particle wave functions, integrated over the momentum $\mathbf{q}$. As this term is nonlocal, it cannot be written in terms of a local spin-isospin transition density, but it requires a nonlocal density matrix. In this term, we have neglected the contribution of the single-particle binding energy to the energy ω_B carried by the virtual meson. The "target excitation" amplitude is obtained from the "projectile excitation" term by interchanging the projectile and target nucleon lines in Fig. 1(a). All of the additional terms in our amplitude are obtained from the amplitude of Fig. 1(a) by interchanging either the initial or final-state nucleon lines.

The third amplitude, given in Fig. 1(c), is obtained from "amplitude A" by exchanging the continuum and bound nucleon lines in the final state. We refer to this term as "amplitude C;" it has the form

$$T_C=-\frac{\sqrt{2}}{3}\frac{f_\pi f_\Delta^2}{m_\pi^3}\int\frac{d\mathbf{q}}{(2\pi)^3}\frac{F(q)\phi_f^\dagger(\mathbf{k}-\mathbf{k}_\pi-\mathbf{q})\phi_i(\mathbf{k}'-\mathbf{q})}{D_\Delta(q_C^\Delta,\omega_C^\Delta)D_\pi(q,\omega_C)}$$
$$\times\langle k'\,|\,\boldsymbol{\sigma}\cdot\mathbf{q}\,|\,i\rangle\langle f\,|\,\mathbf{S}^\dagger\cdot\mathbf{k}_\pi\mathbf{S}\cdot\mathbf{q}\,|\,k\rangle\ , \tag{15}$$

where

$$\omega_C=-\epsilon_i-T_{\mathrm{p}'}\approx-T_{\mathrm{p}'}\ ,$$
$$q_C^\Delta\approx\mathbf{k}_\pi\ , \tag{16}$$
$$\omega_C^\Delta\approx E_\pi+M_{\mathrm{p}}\ .$$

In Eq. (15), several approximations in kinematics have been made. Small bound-state energies and momenta have been dropped in Eq. (16). This simplification allows us to take the isobar propagator outside the integral over $\mathbf{q}$. Like amplitude B, this amplitude is also proportional to a transition density matrix operator.

The final amplitude is obtained by exchanging the bound and continuum nucleon lines in the final state of the "target excitation" amplitude. This term is shown in Fig. 1(d). We refer to this term as "amplitude D," and it has the form

$$T_D=\frac{-\sqrt{2}}{3}\tilde{\rho}_{fi}(\mathbf{q}_A)\frac{f_\pi f_\Delta^2}{m_\pi^3}$$
$$\times F(q_D)\frac{\langle k'\,|\,\boldsymbol{\sigma}\cdot\mathbf{q}_D\,|\,k\rangle}{D_\Delta(q_D^\Delta,\omega_D^\Delta)D_\pi(q_D,\omega_D)}\ , \tag{17}$$

where

$$\mathbf{q}_D=\mathbf{k}'-\mathbf{k}\ ,$$
$$\omega_D=T_{\mathrm{p}'}-T_{\mathrm{p}}\ ,$$
$$\mathbf{q}_D^\Delta\approx\mathbf{k}_\pi\ , \tag{18}$$
$$\omega_D^\Delta\approx E_\pi+M_{\mathrm{p}}\ .$$

In Eq. (18), the same approximations were made, as in Eq. (16). This amplitude, like the "projectile excitation" amplitude, is proportional to a nuclear transition density; the transition density $\tilde{\rho}_{fi}(q)$ which appears in Eq. (17) is a combination of spin-isospin and isospin densities

$$\tilde{\rho}_{fi}(\mathbf{q})=\tfrac{2}{3}\mathbf{k}_\pi\cdot\mathbf{q}\left\langle f\left|\sum_j\tau_j^-\right|i\right\rangle$$
$$-\frac{i}{3}(\mathbf{k}_\pi\times\mathbf{q})\cdot\left\langle f\left|\sum_j\boldsymbol{\sigma}_j\tau_j^-\right|i\right\rangle\ . \tag{19}$$

In general, the transition densities and transition density matrix operators will have considerable dependence upon the spin and angular momentum of the active nucleons. With the simple forms which were chosen for the nuclear wave functions, this sensitivity and selectivity has been lost, so that we may gain a qualitative understanding of these matrix elements. The spin and orbital dependence of this reaction will be explored in a subsequent work.

The c.m. differential cross section is given in terms of the above amplitudes as

$$\frac{d^3\sigma}{d\Omega' d\Omega_\pi dE'}=\frac{10^4}{2(2\pi)^5}\frac{k'k_\pi E'E}{k(1+E/E_A)}\,|\,T_{fi}\,|^2\ . \tag{20}$$

In Eq. (20), the units are μb/sr^2/MeV, and $|\,T_{fi}\,|^2$ is obtained by squaring the sum of the amplitudes of Eqs. (4), (13), (15), and (17), averaging over initial spins and summing over final spins. With our approximations for the momentum dependence of the Δ propagator, and with the simple Gaussian wave functions and transition densities which we have employed, then the PW cross sections can be reduced to a sum of terms requiring no more than a single integral. The form of the final equations, and the expressions which were integrated, are listed for completeness in Appendix A.

III. RESULTS AND DISCUSSION

A. General features of reaction amplitudes

We have calculated the cross sections in coplanar geometry; i.e., where the incident and outgoing particles all lie in a plane in the c.m. system. As the spin dependence of this interaction is not investigated, there is little additional information obtained by going out of plane. In the calculated cross sections, the c.m. angle between the incident and outgoing protons is kept fixed at $-10°$ relative to the incident direction. The geometry chosen for this paper is shown schematically in Fig. 3, where the incident and scattered proton directions are shown in the c.m. system. Looking down on the reaction plane, angles are defined as negative if they occur to the right of the incident beam direction, and positive if they occur to the left of the incident proton direction. Thus a negative pion angle means that the pion and proton come out on the same side, and a positive pion angle means that the pion and proton come out on opposite sides in the reaction plane. The kinematics are appropriate for a target with mass $A=16$.

In Fig. 4 the differential cross section is shown for

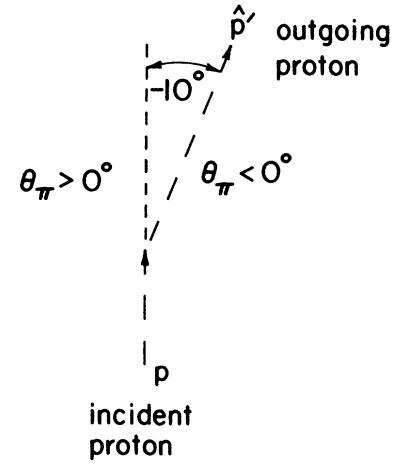

FIG. 3. Geometry for reaction cross sections. Calculations are done in coplanar geometry. Angles are defined as negative if they are to the right of the incident direction, and positive if they are to the left. The outgoing proton direction is fixed at a c.m. angle of $-10°$ in this notation.

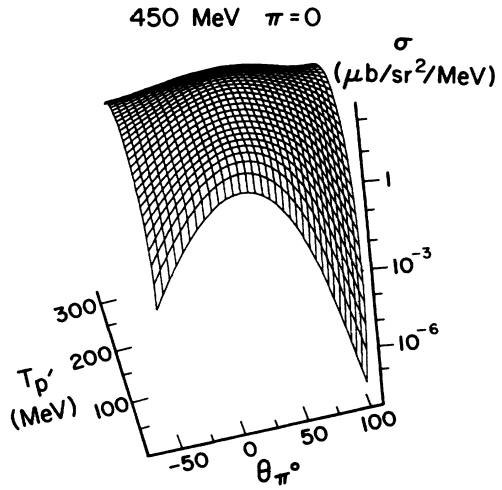

FIG. 4. Cross section for the reaction $(p,p'\pi^+)$ leading to a neutron particle-proton hole relative to an inert core. The cross section, in $\mu b/sr^2/MeV$, for proton incident kinetic energy 450 MeV vs pion c.m. angle in degrees, and outgoing proton kinetic energy in MeV. No self-energy effects are included for either the intermediate pion or isobar, and cross sections are calculated using plane waves for the continuum protons and the pion.

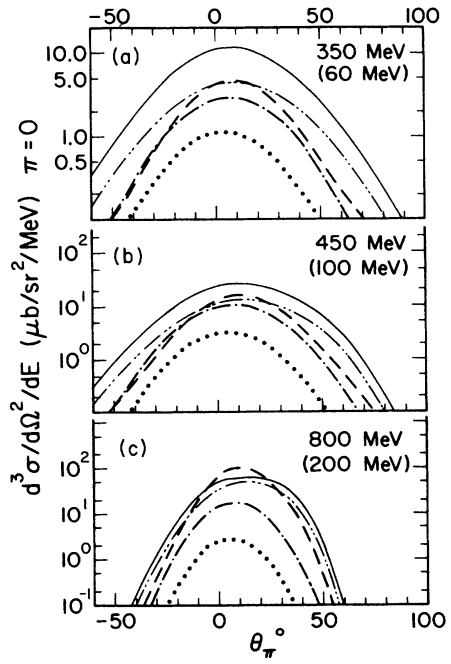

FIG. 5. Differential cross sections, in $\mu b/sr^2/MeV$, vs c.m. angle for the outgoing pion. (a) Incident proton energy 350 MeV, and outgoing proton energy 60 MeV; (b) incident energy 450 MeV and outgoing energy 100 MeV; (c) incident energy 800 MeV and outgoing energy 200 MeV. Solid curve, full differential cross section; dashed curve, result using only amplitude A of Fig. 1; dot-dot-dashed curve, result using amplitude B; dotted curve, result using only amplitude C; dot-dashed curve, result using only amplitude D of Fig. 1. Results are shown in PW approximation with no self-energy effects included.

$(p,p'\pi^+)$ for incident proton kinetic energy 450 MeV. The three-dimensional plot shows the cross section as a function of the kinetic energy of the outgoing proton, and the c.m. scattering angle of the pion. The cross section has been calculated in the plane-wave (PW) approximation, using free propagators for both the intermediate pion and isobar. It can be seen that there is a broad peak in the calculated cross section, corresponding to $\theta_\pi \approx +10 \rightarrow +20°$. The magnitude of the peak cross section varies slowly as the proton kinetic energy changes. The cross section falls off monotonically as the pion angle is varied away from the peak.

In Fig. 5, the cross sections are shown as a function of the outgoing pion angle, for fixed outgoing proton kinetic energy. Figure 5(a) shows the cross section for an incident energy of 350 MeV and outgoing energy 60 MeV, Fig. 5(b) is for incident energy 450 MeV and outgoing energy 100 MeV, and Fig. 5(c) is for incident energy 800 MeV and outgoing energy 200 MeV. For each incident energy, the outgoing proton energies are chosen to correspond to the overall peak in the cross section.

The solid curve gives the full cross section; the other curves show the cross section for each amplitude separately. While the contribution from amplitude "C" is smaller than the others, the remaining amplitudes contribute about equally to the cross section. The cross section has a broad peak for a small positive value of θ_π corresponding to the minimum momentum transfer available in the reaction, and the cross section decreases monotonically as the angle is varied with respect to the maximum. The width and shape of the cross section peak are determined by the nuclear wave functions and transition densities. The maximum cross section increases somewhat as the proton energy increases. At 350 MeV, the peak cross section is about 10 $\mu b/sr^2/MeV$, whereas at 800 MeV, the peak cross section is roughly 60 $\mu b/sr^2/MeV$.

Figure 6 shows the outgoing proton energy spectrum for fixed pion angle of $+10°$, and incident proton energies 350, 450, and 800 MeV. We find that, as a function of $T_{p'}$, the energy distributions for amplitudes A and B differ from those of C and D; compared to C and D, the former pair peaks at a considerably smaller value of $T_{p'}$, and the separation between peaks increases with incident energy T_p. This feature helps to separate contributions from two classes of diagrams.

Figure 6 is plotted for a pion angle very near the peak of the cross sections; for such an angle, the nuclear momentum transfer does not change very much as the outgoing proton energy is varied. As a result, the nuclear transition densities are relatively constant, hence the quantity which varies most rapidly with outgoing proton energy is the Δ propagator. For amplitudes C and D, the Δ propagator has the form

$$D_\Delta \approx \frac{1}{\delta M + T_\Delta - (T_p - T_{p'}) + i\Gamma/2}\ , \tag{21}$$

where $\delta M \equiv M_\Delta - M_N$. The maximum in this term occurs when the real part of the denominator has a minimum, i.e., for $T_{p'} \approx T_p - \delta M$. In Fig. 6, amplitudes C and D peak at this value of $T_{p'}$. For the terms A and B,

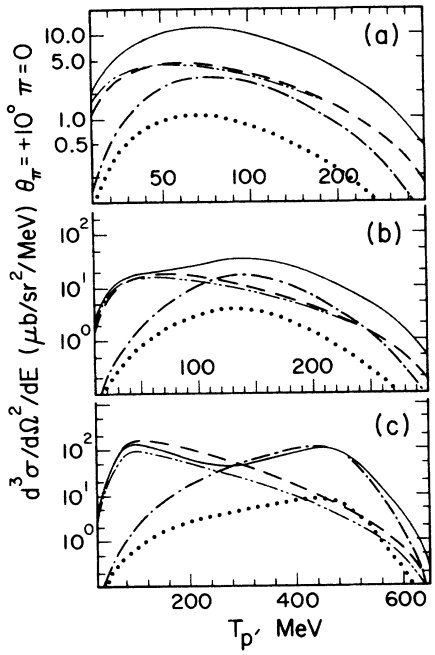

FIG. 6. Differential cross sections vs outgoing proton kinetic energy, with c.m. pion angle fixed at $+10°$. (a) Incident proton kinetic energy 350 MeV; (b) incident energy 450 MeV; (c) incident energy 800 MeV. All other conditions are the same as for Fig. 5.

the Δ propagator is

$$D_\Delta \approx \frac{1}{\delta M + (\mathbf{k}'+\mathbf{k}_\pi)^2/2M_\Delta - T_p + i\Gamma/2} . \tag{22}$$

Again, the maximum in this term occurs when the real part of the denominator is smallest. In contrast to Eq. (21), this occurs at a smaller value of $T_{p'}$. For proton incident energies of 350, 450, and 800 MeV, the real part of Eq. (22) has a minimum at $T_{p'}=40$, 50, and 100 MeV, respectively. From Fig. 5, this is just where amplitudes A and B reach their maximum values. This analysis also explains the increased separation in the two peaks as the incident energy increases.

The two ways we have chosen to view the cross sections give us quite different information about the reaction. Fixing the outgoing kinetic energy and varying the pion angle gives direct information regarding the shape of the nuclear transition densities. On the other hand, if the pion angle is fixed around the maximum of the cross sections, the resulting proton energy spectrum allows a separation of the cross section into different reaction amplitudes.

B. Medium effects on the pion

In the previous section, the (p,p'π^+) cross sections were calculated using free meson and isobar propagators. In this section, we calculate the effects arising from modification of the pion propagation due to the nuclear medium. We will estimate the effects of particle-hole and Δ-hole excitations produced by a propagating pion. These contributions to first order are shown in Fig. 7(a)

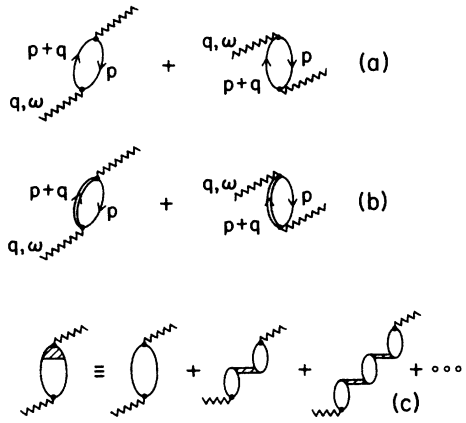

FIG. 7. Contributions to meson self-energy. (a) Direct and exchange particle-hole contributions to self-energy; (b) direct and exchange isobar-hole contributions to self-energy; (c) renormalization of direct particle-hole self-energy by including short-ranged repulsion in particle-hole interaction. Short-ranged term is shown as the shaded line, and is summed to all orders in the "ring approximation."

(the particle-hole contribution) and Fig. 7(b) (the Δ-hole contribution). The full meson propagator is then given by

$$G(q,\omega) = \frac{G_0(q,\omega)}{1 - G_0(q,\omega)\Pi^0(q,\omega)} , \tag{23}$$

where the free propagator G_0 has the form

$$G_0(q,\omega) = (\omega^2 - q^2 - m^2 + i\eta)^{-1} . \tag{24}$$

In Eq. (23), Π^0 is the self-energy of the pion. For a real pion Π^0 is related to the optical potential through $\Pi^0 = 2\omega V_{\rm opt}$.

To calculate the self-energies, we approximate the nuclear density distribution by a Fermi gas, for which the expressions are well known.[19,24,25] They are summarized in Appendix B. The self-energy from the particle-hole amplitudes of Fig. 7(a) is given in Eq. (B3), while Eq. (B7) gives the contribution from the isobar-hole amplitudes of Fig. 7(b). The Fermi momentum has been chosen as $k_F = 210$ MeV/c, and the nucleon effective mass is taken as $M^* = 0.7 M_N$. Inserting the self-energies Π^0 into the propagator of Eq. (23) sums the ring diagrams for pion propagation in the nuclear medium.

Figure 8 shows a three-dimensional view of the cross section versus the outgoing proton kinetic energy and the pion angle. This can be compared with Fig. 4, in which the pion self-energy is not included. The "spikes" in Fig. 8 represent poles in the cross section. The self-energy effects are so large that they produce zeroes in the denominator of the pion propagator at certain momentum transfers; in PW approximation, this produces a pole in the cross section.

In general, the self-energies $\Pi^0(q,\omega)$ are complex.

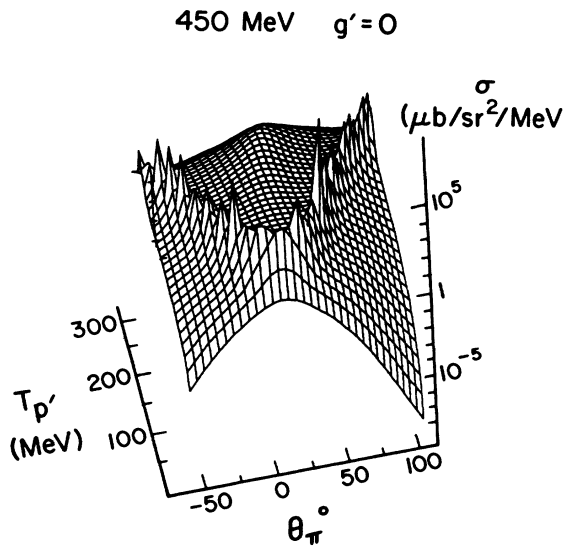

FIG. 8. Differential cross section for incident proton kinetic energy 450 MeV. Conditions are the same as for Fig. 4, except that the intermediate pion self-energy is included, with Migdal parameter $g'=0$. In PW approximation, the spikes in this diagram correspond to poles in the differential cross section.

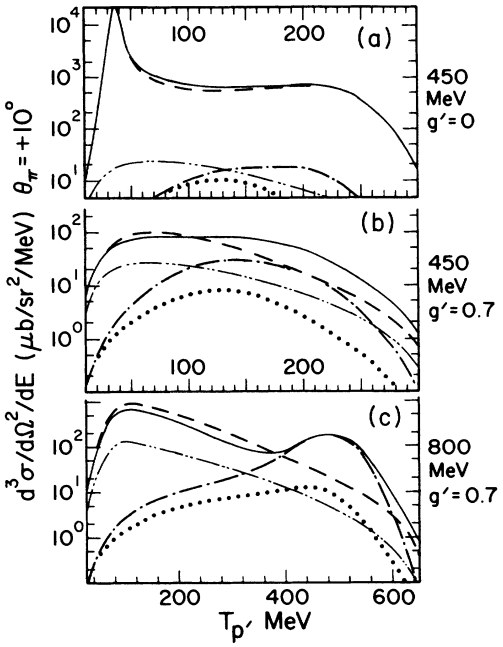

FIG. 9. Differential cross section vs outgoing proton kinetic energy, with pion c.m. angle fixed at $+10°$. (a) Incident proton kinetic energy 450 MeV and Migdal parameter $g'=0$; (b) incident energy 450 MeV and $g'=0.7$; (c) incident energy 800 MeV and $g'=0.7$. Description of the curves is the same as in Fig. 5.

However, for $\omega=0$, as is the case for amplitude A, the self-energy is real, as can be seen from Eq. (B6). As a result, the self-energy can produce a pole in the pion propagator for amplitude A, while for all other amplitudes it produces both a real and an imaginary part. In Fig. 9(a), the cross section at 450 MeV is plotted for pion c.m. angle $+10°$. The cross section from each amplitude is plotted separately; it is clear that the pole arises from amplitude A, which completely dominates the contribution from all other amplitudes.

While the self-energy effects will give a considerable increase in the calculated cross sections, the poles in amplitude A are unphysical. These poles are just the "pion condensate" seen in early calculations of the pion polarization potential in nuclei.[16,17,26] As is well known, this condensate occurs because the particle-hole and isobar-hole interactions in this approximation are strongly attractive at short distances. In reality, we should also include the strong short-ranged repulsion which arises from exchange of heavier mesons and other many-body effects; when this is done, the spurious poles in the full Green function disappear. The distortion of the continuum particles, which has been neglected here, would also "soften" the poles which appear in the PW limit.

In order to estimate the effects of the short-ranged repulsion, we introduce the Migdal parameters, which are supposed to mock up the complicated density-dependent effective interaction between particles and holes in the nuclear medium. The additional short-range piece has the form

$$W_{ph}=\frac{f_\pi^2}{m_\pi^2}g'\boldsymbol{\sigma}_1\cdot\boldsymbol{\sigma}_2\boldsymbol{\tau}_1\cdot\boldsymbol{\tau}_2+\frac{f_\Delta^2}{m_\pi^2}g'\mathbf{S}_1^\dagger\cdot\mathbf{S}_2\mathbf{T}_1^\dagger\cdot\mathbf{T}_2 + \frac{f_\pi f_\Delta}{m_\pi^2}g'_{N\Delta}[\mathbf{S}_1\cdot\boldsymbol{\sigma}_2\mathbf{T}_1\cdot\boldsymbol{\tau}_2+\text{H.c.}]\ . \tag{25}$$

When all rings with short-ranged correlations in intermediate states are summed, as shown diagrammatically in Fig. 7(c), the self-energies are renormalized. If the self-energies are written in terms of the "susceptibilities" as

$$\Pi_N\equiv -q^2\chi_N\ , \qquad \Pi_\Delta\equiv -q^2\chi_\Delta\ , \tag{26}$$

then the susceptibilities get renormalized to

$$\chi_N\rightarrow\frac{1+\chi_\Delta(g'_{N\Delta}-g')}{(1+g'\chi_\Delta)(1+g'\chi_N)-(g'_{N\Delta})^2\chi_N\chi_\Delta}\chi_N(q,\omega)\ , \tag{27}$$

$$\chi_\Delta\rightarrow\frac{1+\chi_N(g'_{N\Delta}-g')}{(1+g'\chi_\Delta)(1+g'\chi_N)-(g'_{N\Delta})^2\chi_N\chi_\Delta}\chi_\Delta(q,\omega)\ .$$

For our calculations, we have chosen $g'_{N\Delta}=g'$, in which case the renormalization equations become

$$\chi_N(q,\omega)\rightarrow\frac{\chi_N(q,\omega)}{1+g'(\chi_N+\chi_\Delta)}\ , \qquad \chi_\Delta(q,\omega)\rightarrow\frac{\chi_\Delta(q,\omega)}{1+g'(\chi_N+\chi_\Delta)}\ . \tag{28}$$

Most estimates of these quantities give a Migdal parameter between $0.5\le g'\le 1$ for the πNN coupling. For the πNΔ case, there is much less certainty;[16] for example, Arima *et al.*[27] obtain a value $g'_{N\Delta}\approx 0.3$, which value is

also preferred in an analysis of the ^{6}Li(p,Δ^{++})^{6}He reaction by Jain.[28] However, $g'_{N\Delta}=g'$ is a common choice, given the uncertainty in this quantity.

Figure 9 shows the effects of the short-range repulsion in the particle-hole and isobar-hole terms. The cross sections are plotted for pion angle + 10°, versus the outgoing proton kinetic energy. Figures 9(a) and (b) show the cross section for incident energy 450 MeV and Migdal parameters $g'=0$ and $g'=0.7$, respectively. For $g'=0.7$, it is clear that the pole in the cross section which dominates Fig. 9(a) has completely disappeared. However, inclusion of the renormalized self-energy increases amplitude A relative to the other amplitudes, and it also increases the overall cross sections relative to the calculation without the pion self-energy. In our calculation, the self-energy $\Pi^0(q,\omega)$ is enhanced considerably in the region $\omega\approx 0$, and for $q\approx 1-3$ fm^{-1}; thus inclusion of the self-energy produces a much larger effect on amplitude A than on any other amplitude.

From Fig. 9(b), for low values of the outgoing kinetic energy $T_{p'}\leq 150$ MeV, the contribution from amplitude A (the dashed curve in Fig. 9) dominates the cross sections. Figure 9(c) shows the cross sections for incident energy 800 MeV and $g'=0.7$; for outgoing kinetic energy $T_{p'}\leq 350$ MeV, the cross sections are dominated by amplitude A; above this energy, the amplitudes are dominated by amplitude D (the dot-dashed curve).

Figure 10 shows the effects of the renormalized pion self-energy on the proton energy spectrum. Figure 10(a) shows the energy spectrum for proton incident energy 450 MeV and pion angle + 10°. The dot-dashed curve is the result with no self-energy, the dashed and solid curves are the results with Migdal parameters $g'=0.7$ and $g'=0.5$, respectively. In Fig. 10(b) the same results are shown for proton incident energy 800 MeV. First, the cross section is enhanced by a large amount relative to the case with no self-energy; there is an increase of a factor of five at 450 MeV and about eight at 800 MeV (for proton kinetic energy below 400 MeV). Second, the self-energy effect primarily enhances the "projectile excitation" amplitude: for large outgoing proton kinetic energy, where the contribution from Fig. 1(d) is important, the self-energy produces only a slight increase in the cross section; this is especially noticeable for the 800 MeV results. The two curves in Fig. 9 corresponding to different values of g' differ by about 60% at the peak cross sections, and they differ by about 20% at the highest values of $T_{p'}$. This gives a measure of the variation in the cross-sections arising from the uncertainty in the precise value for g'.

The present calculation is a nonrelativistic treatment of the (p,p'π^+) reaction. For one aspect of this model—the pion self-energy—a direct comparison could be made between relativistic and NR calculations. Dmitriev and Suzuki[29] have carried out a relativistic calculation of the pion self-energy. In Appendix C, this calculation is reviewed and compared with the NR result. As can be seen from Fig. 14 in Appendix C, there are no substantial differences between the relativistic and nonrelativistic treatments of the pion self-energy, for a proton incident energy of 450 MeV.

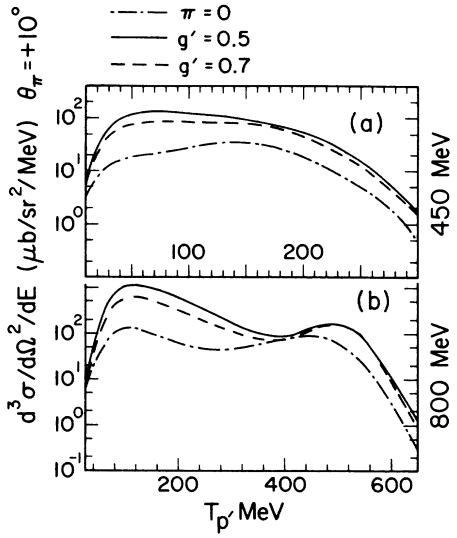

FIG. 10. Dependence of the cross sections on the pion self-energy, and on the choice of the Migdal parameter. Dot-dashed curve, self-energy zero; solid curve, $g'=0.5$; dashed curve, $g'=0.7$. Cross sections vs outgoing proton energy for pion angle + 10°. (a) Incident energy 450 MeV; (b) incident energy 800 MeV.

The zero-ranged "contact term" of Eq. (25) mocked up the short-ranged repulsion in the particle-hole interaction; this term produced a significant effect on the pion self-energy. This term could also be included directly at the isobar-production vertex; i.e., in addition to the one-meson-exchange amplitude of Fig. 1(a) we could also include a contact term of the form

$$H_{ZR}=\frac{f_\pi f_\Delta}{m_\pi^2}g'_{N\Delta}(\mathbf{S}_1\cdot\boldsymbol{\sigma}_2\mathbf{T}_1\cdot\boldsymbol{\tau}_2+\text{H.c.})\ . \tag{29}$$

Such a term is shown schematically in Fig. 11(a), where the circle labeled g' represents the zero-ranged force of Eq. (29). It is straightforward to show that, due to the antisymmetrization between continuum and bound nucleons, addition of such a term would have no effect upon our calculated cross sections. The reason for this is straightforward. Indistinguishability between nucleons

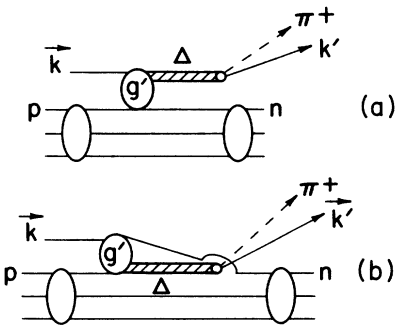

FIG. 11. Contribution of short-ranged force in the NN→NΔ interaction, for the (p,p'π^+) reaction. (a) This amplitude corresponds to the term in Fig. 1(a); (b) this term corresponds to the term in Fig. 1(b). For a zero-ranged force such as the Migdal interaction, these two terms cancel completely.

requires that, in addition to the zero-ranged term of Fig. 11(a), we should also include an exchange term, shown schematically in Fig. 11(b). For zero-ranged interactions, the two terms of Fig. 11 give equal and opposite contributions and thus cancel completely. The zero-range terms corresponding to Figs. 1(c) and (d) also cancel completely.

Alons *et al.*,[7] and Iqbal and Walker,[5] have found a similar result for (p,π) reactions. They find that including a zero-ranged term (which gives a four-point function for the $NN \rightarrow N\Delta$ amplitude) gives no contribution to their overall reaction amplitudes. They also find that including a ρ meson instead of a pion gives a very small contribution. For the ρ there is a large, but not complete, cancellation between direct and exchange terms. Similar results have been found by Santra and Jain for the (p,Δ^{++}) reaction.[30] We also expect a large cancellation between terms if the ρ-meson contribution were included in our amplitudes. For this reason, contributions from ρ mesons or other heavy mesons have not been included in our calculation.

C. Medium effects on the Δ

In the previous section, nuclear medium effects were found to produce a significant change in the pion propagator. It is likely that isobar propagation will also be altered considerably by the nuclear medium. There have been many estimates of nuclear effects on intermediate isobars. The most prominent of these has been the isobar-hole approach,[15] which has been applied extensively to production and propagation of isobars in pion elastic and inelastic scattering, and pion-induced total cross sections. In addition, several groups have calculated nuclear effects on intermediate isobars in (p,π) reactions and other processes.[5,16,31] The estimates presented in this paper are considerably less rigorous, as we wish to get only a rough idea of the size of the effects in the $(p,p'\pi^+)$ reaction. The qualitative results from more detailed calculations will be used to estimate the isobar medium effects.

The qualitative modifications of the Δ are expected to be of two types: first, we expect a shift in the position of the Δ peak. Second, we expect a modification of the isobar width in the medium. Changes in the isobar width arises from two competing mechanisms. First, Pauli effects in intermediate transitions inhibit the process $\Delta \rightarrow N + \pi$ as some of the nucleon states are occupied; this is shown schematically in Fig. 12(a). Such effects tend to decrease the isobar width in the medium relative to the free width $\Gamma_0 = 116$ MeV. The other contribution to the width arises from nuclear interactions of the isobar; a typical transition is shown to first order in Fig. 12(b). Such "spreading" transitions[15] produce both a shift in the position of the Δ peak, and a change in the isobar width in the medium. In the vicinity of the isobar resonance, a reasonable local estimate for the real part of the "spreading potential" is a 35-MeV attraction.[32] The imaginary part of the spreading potential tends to increase the width of the isobar, at least in the vicinity of the isobar resonance. The two effects on the width differ somewhat, as the Pauli effect goes roughly as the nuclear density and the "spreading" effects go crudely as the square of the density; nevertheless, there is considerable cancellation between the two effects.

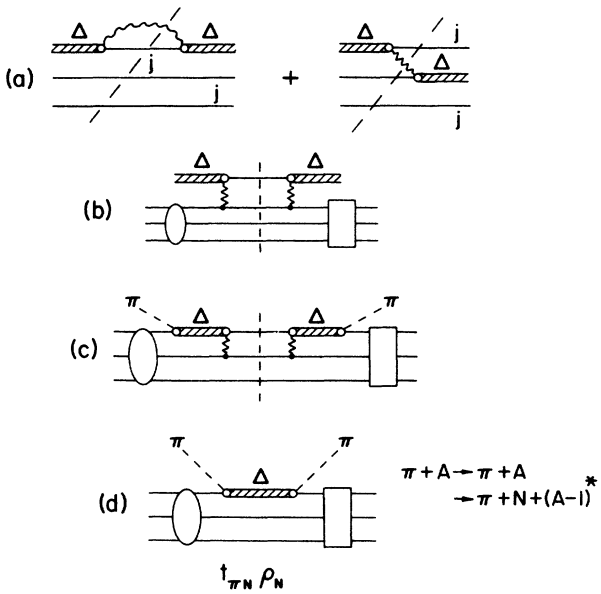

FIG. 12. Contributions to the isobar self-energy, and to the distortions in pion final-state interactions. (a) Pauli-blocked terms in isobar-nucleus interactions. The index "j" means that the particular nucleon state is already filled. (b) One contribution to the isobar spreading width: virtual transitions into high-lying nucleon-only states. In this figure, circles refer to bound nuclear states, and rectangles denote either bound or continuum states. (c) One contribution to absorption from scattering of final-state pion. Pion produces an isobar on a target nucleon, and then a transition occurs to nucleonic intermediate states. Note that the intermediate state in (c) is identical to the state produced in (b). (d) Contributions of final-state pion scattering in the "$t\rho$" approximation. Intermediate states contribute through both elastic scattering and single-nucleon knockout.

For the Pauli effects, a distinction has been made between the amplitudes A and B, and the amplitudes C and D. In the former case, the isobar carries considerably more energy (the sum of the final proton and pion total energies) than in the latter case, when the isobar carries the pion energy and proton rest mass. Changes in the isobar width in the medium have been parametrized by replacing the free width in the isobar denominator by

$$\Gamma_0 \rightarrow P\Gamma_0 + \Gamma_A \tag{30}$$

where P represents the suppression of isobar decays in the medium due to Pauli effects, and Γ_A gives the "absorption width" due to isobar-nucleus collisions. The Pauli suppression should be considerably larger for amplitudes C and D, relative to amplitudes A and B. We have chosen $P=1$ for amplitudes A and B (i.e., Pauli effects are neglected for these two amplitudes), and $P=0.7$ for amplitudes C and D.

The absorption width has been calculated through the spreading width $\Gamma_A = g\Gamma_S$, where the spreading width is chosen as $\Gamma_S = 70$ MeV. This value is somewhat higher

than the values deduced from pionic atoms,[33] and slightly lower than the spreading width deduced from pion scattering.[15] The factor g is added to account for the fact that in our calculations the isobar is produced preferentially near the nuclear surface. This factor represents the fraction of the central nuclear density, in the region where the isobar is formed. We have chosen $g=0.7$ for our calculations.

Figure 13 shows the results obtained when the isobar propagator is modified. The curves correspond to a proton incident energy of 450 MeV. The pion self-energy has been included with Migdal parameter $g'=0.7$. The solid curve corresponds to Pauli effects only, i.e., both the real and imaginary spreading potential zero. The dashed curve includes in addition a real spreading potential of -35 MeV, and the dot-dashed curve includes a further absorption width $g\Gamma_S=49$ MeV. Relative to the case with Pauli effects only, inclusion of the real spreading potential produces roughly a factor of two increase in the cross section, while including the spreading width results in a decrease of approximately 60% in the cross section. These effects are smaller than the estimated pion self-energy corrections, and the net result from both Pauli corrections and the spreading potential is less than a factor of two change in the overall cross sections. These are qualitative estimates of the size and energy dependence of the isobar effects, which could be expected from a more quantitative calculation of the propagation of a Δ in the nuclear environment. Nevertheless, it is clear that the net result of all isobar medium effects is only a small change, and much smaller than the medium polarization effects which have been estimated for the intermediate pion.

D. Final-state interaction effects

Thus far we have calculated the (p,p'π) cross sections in a plane-wave approximation, which neglects the proton-nucleus and pion-nucleus interactions. The nuclear interactions generally produce both absorptive and dispersive effects, and both can be expected to be important. However, for the large incident energies treated in this calculation, the most important effects are likely to be the absorption effects, and qualitative estimates of these effects are provided in this section.

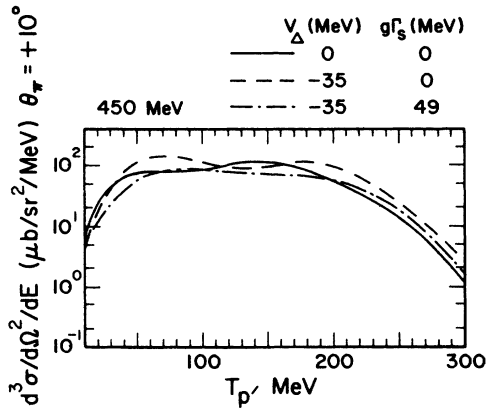

FIG. 13. Effects of isobar self-energy on cross sections. Incident energy 450 MeV and pion angle + 10° vs outgoing proton energy. Pion self-energy is included with $g'=0.7$. Solid curve, $V_\Delta=0$ and $g\Gamma_s=0$ (i.e., only Pauli blocking is included for the Δ); dashed curve, $V_\Delta=-35$ MeV and $g\Gamma_s=0$; dot-dashed curve, $V_\Delta=-35$ MeV and $g\Gamma_s=49$ MeV.

We use the eikonal approximation to estimate the attenuation factor for a particle travelling through a medium. First, we associate a refractive index $n(r,E)$ with the nuclear medium, and we factorize the energy and radial dependence as

$$n(r,E)=n(E)\frac{\rho(r)}{\rho_0}\ , \tag{31}$$

where ρ is the nuclear density distribution, and

$$n(E)=\frac{\kappa(E)}{k(E)}\ . \tag{32}$$

Here k is the external wave number, and κ is the wave number in the medium. The imaginary part of this refractive index is defined as n_0. In terms of n_0, the attenuation factor can be written as

$$\eta(E)=\int d\mathbf{b}\,dz\frac{\rho(\mathbf{b},z)\exp[-kn_0(E)L(b)]}{\int d\mathbf{b}dz\rho(\mathbf{b},z)}\ , \tag{33}$$

where $L(b)$ is the length of path travelled by the particle in the medium. This length is given by

$$L(b)=\int_0^\infty \frac{\rho(r)}{\rho_0}dz\ . \tag{34}$$

The integration can be done analytically if the nucleon density is approximated by a Gaussian $\rho(r)=\rho_0\exp(-r^2/\alpha^2)$, in which case the attenuation factor has the form

$$\eta(E)=\frac{1-\exp[-\sqrt{\pi}\alpha kn_0(E)]}{\sqrt{\pi}\alpha kn_0(E)}\ . \tag{35}$$

Once the value of n_0 is known, the attenuation due to the medium can be calculated. For protons, $n_0(E)$ is obtained from the imaginary part of the optical potential W_0,

$$n_0(E)=\frac{E}{k^2}W_0(E)\ . \tag{36}$$

For pions n_0 is calculated using the method of Ericson and Hüfner.[34] κ, the pion wave number in the medium, is determined from the dispersion relation

$$\kappa^2=k^2+4\pi\rho f_{\pi N}(\kappa,E) \tag{37}$$

where $f_{\pi N}$ is the π-N scattering amplitude for the effective pion-nucleon interaction.

For the (N,π) reaction treated in the isobar-hole model, Hirata[35] has argued that the effective pion-nucleon interaction $f_{\pi N}$ should be the nonresonant interaction, the resonant piece having been included in the isobar-nucleus interaction. Calculations have been carried out on ^{4}He (Ref. 36) and ^{16}O (Ref. 37) using this approach. Our model differs from those since, for two of the amplitudes

considered (A and B), the isobar decays to a free proton and free pion. This produces a spectrum of final pion energies, so that the pion-nucleus energy varies over a wide range. Also for two amplitudes (A and C) the intermediate isobar is produced by exciting the projectile and not one of the target nucleons. As a result, some of the resonant pion-nucleon amplitude should be included in constructing the final pion-nucleus interaction.

In this calculation, the pion-nucleon amplitude used to construct the pion-nucleus final-state interaction is the resonant amplitude f_{33}. For the projectile excitation amplitude A, this will not involve significant double counting. However, for some of the other amplitudes, including both the isobar-nucleus interaction and the resonant term in the pion-nucleus interaction would involve considerable multiple counting. For this reason, the attenuation effects calculated here will be applied only to the peak cross sections. For the specific kinematics at which the attenuation is estimated, the dominant term in these calculations comes from amplitude A; the approximations used here should be valid for this term.[38]

Since the pion-nucleon interaction is being approximated by the (3,3) amplitude, an accurate expression for π^+ scattering from a symmetric nucleus is

$$f_{\pi+\mathrm{N}}=\tfrac{1}{2}(f_{\pi+\mathrm{n}}+f_{\pi+\mathrm{p}})\approx\tfrac{2}{3}f_{33}\ . \tag{38}$$

Using a Breit-Wigner resonant form for the amplitude f_{33} gives

$$f_{\pi+\mathrm{N}}\approx\frac{c\kappa^2}{E-E_R+\frac{1}{2}i\Gamma}\ ,$$
$$c\equiv-(\tfrac{2}{3})\frac{58a^3}{1+(ka)^2}\ , \tag{39}$$

where $a=1.24$ fm is the interaction radius. The effective width of the isobar is given by $\Gamma=P\Gamma_0$, where Γ_0 is the free width, and $P=0.7$ estimates the effect of Pauli blocking on the width of the isobar in the nucleus. Using these expressions, the refractive index $n_0(E)$ for pions is given by

$$n_0(E)=\frac{\Delta\Gamma/4}{(E-E_R+\frac{3}{4}\Delta)^2+\frac{1}{4}\Gamma^2}\ ,$$
$$\Delta\equiv4\pi\rho_0 c\ . \tag{40}$$

The dispersion relation (37) is equivalent to an optical potential approach, if the optical potential is defined through the folding of the π–N t matrix with the nuclear density. Tandy *et al.*[39] have shown that such optical potentials contain nucleon knock-out as the primary reactive content. Therefore, the main contribution to $n_0(E)$ in Eq. (40) is the nucleon knock-out channel ($\pi^+,\pi^+\mathrm{N}$). Furthermore, since the π–N t matrix has been approximated by the (3,3) amplitude, dynamically the nucleon knock-out is mediated by a $\Delta(1232)$ in the intermediate state. The pion absorption for this n_0 occurs through the process

$$\pi^+ + [\mathrm{N}+(A-1)]\rightarrow\Delta+(A-1)^*\rightarrow\pi^+ +\mathrm{N}+(A-1) \tag{41}$$

which is shown schematically in Fig. 12(d).

In addition to nucleon knock-out, pion flux is also lost through real absorption in the medium. One term which contributes to real absorption in the final-state interaction is shown in Fig. 12(c). In this model, real absorption is estimated by adding to n_0 of Eq. (40) an additional term, n_A due to real absorption. It is assumed that the main contribution to n_A arises from the virtual process $\Delta\mathrm{N}\rightarrow\mathrm{NN}$; n_A is estimated from the spreading width discussed in the previous section; we used

$$n_A=\frac{E_\pi}{2k_\pi^2}g\Gamma_s\ , \tag{42}$$

where the value of the absorption width was taken as $g\Gamma_s=49$ MeV.

The same questions of double counting arise for real absorption as for the pion scattering term described earlier. In the final-state interaction, real absorption arises from production of an isobar on one of the target nucleons and the intermediate process $\Delta\mathrm{N}\rightarrow\mathrm{NN}$, as shown schematically in Fig. 12(c). However, the isobar spreading width, discussed in the previous section, arises from the same process as shown in Fig. 12(b). In treating the contribution due to real absorption, either the spreading width has been included in the isobar propagator, or real absorption has been included in the attenuation of the final pion, but it has not been included in both places. The real absorption has thus been underestimated. How-

TABLE I. Pion attenuation.

		Knock-out			Knock-out + real absorption		
T_π (MeV)	Γ_f (MeV)	n_0	$\lvert\eta_L\rvert^{-2}$	$\lvert\eta_H\rvert^{-2}$	n_0	$\lvert\eta_L\rvert^{-2}$	$\lvert\eta_H\rvert^{-2}$
50	24.4	0.073	1.2	1.4	0.355	2.7	4.8
100	56.5	0.243	2.8	5.0	0.398	4.9	10.6
150	87.6	0.516	11.1	28.1	0.626	15.7	41.2
200	116.0	0.260	5.2	11.4	0.347	8.0	19.2
250	116.0	0.094	2.2	3.4	0.166	3.6	7.1
300	116.0	0.037	1.4	1.8	0.100	2.5	4.2
350	116.0	0.018	1.2	1.4	0.072	2.2	3.3
400	116.0	0.009	1.1	1.2	0.058	2.0	3.0
500	116.0	0.004	1.0	1.1	0.044	1.9	2.7
600	116.0	0.002	1.0	1.0	0.036	1.8	2.6

TABLE II. Total attenuation.

T_p (MeV)	$T_{p'}$ (MeV)	T_π (MeV)	n_0(p)	n_0(p')	Knock-out no real absorption $\lvert\eta_L\rvert^{-2}$	Knock-out no real absorption $\lvert\eta_H\rvert^{-2}$	Knock-out + real absorption $\lvert\eta_L\rvert^{-2}$	Knock-out + real absorption $\lvert\eta_H\rvert^{-2}$
350	50	160	0.050	0.082	24.4	65.2	31.4	84.7
450	100	210	0.046	0.063	15.2	39.7	20.5	54.5
800	250	410	0.049	0.027	6.7	15.6	9.8	24.3

ever, in Tables I and II, the two methods for including real absorption can be compared with one another.

Table I lists the pion-nucleus attenuation factor $\lvert\eta\rvert^{-2}$ for various pion energies. For each pion energy, the pion refractive index n_0 of Eq. (40) is listed, and representative values of the attenuation are tabulated (these numbers give the amount by which the cross section is decreased relative to a PW calculation). η_L gives the attenuation expected for a pion of this kinetic energy traversing a light nucleus [$\alpha=2.73$ fm in Eq. (35), the charge radius of ^{16}O)], and η_H gives the attenuation for a heavy nucleus ($\alpha=4.5$ fm). In the columns labeled "knock-out," only the nucleon knock-out is included in calculating the refractive index; in the columns labeled "knock-out plus real absorption," both knock-out and real pion absorption are included. Depending on the target nucleus and the energy, attenuation can range from a factor of 10–40.

In order to determine the total reduction factor for the (p,p'π^+) reaction, the total attenuation due to both the protons and the pion has been estimated by replacing the factor kn in Eq. (35) with

$$kn \rightarrow k_\pi n_0(E_\pi)+k_p n_0(E_p)+k_{p'} n_0(E_{p'}) . \quad (43)$$

Table II lists the total reduction factors for three values of the incident proton kinetic energy: 350, 450, and 800 MeV. The kinetic energies for the outgoing protons are taken to coincide with the peak cross sections at each incident energy; the resulting outgoing energies are 50, 100, and 250 MeV, respectively. The values of the outgoing pion energy are then fixed by the kinematics. For proton energies below 300 MeV, the imaginary part of the proton-nucleus optical potential is taken from proton scattering data.[40] Above 300 MeV the imaginary optical potential is obtained from the high-energy relation

$$W_0(E)=\frac{k\sigma_T\rho_0}{2E} , \quad (44)$$

TABLE III. Effects of final-state interactions on calculated cross sections.

T_p (MeV)	$T_{p'}$ (MeV)	$\sigma_{peak}(\mu b/sr^2/MeV)$ a	b	x
350	50	50.3	1.6	1.4
450	100	116	5.7	5.7
800	250	331	34.1	40.6

[a]No pion-attenuation, no Γ_A in Δ.
[b]Knock-out + real pion absorption, no Γ_A in Δ.
[c]Knock out in pion and Γ_A in Δ.

where σ_T is the total NN cross section.[41] Again, the results are given for knock-out effects alone and knock-out plus real absorption, for both light and heavy nuclei.

From Tables I and II, inclusion of real absorption of the final-state pion reduces the cross sections by about 40%. In the previous section, it was found that inclusion of the imaginary spreading potential in the isobar propagator decreased the peak cross sections by about 60% (compare the dashed and dot-dashed curves in Fig. 13). The two methods of estimating the effects of real pion absorption thus produce similar reductions in the calculated cross sections.

Table III shows the calculated peak cross sections with and without the attenuation factor, for the three energies listed in Table II. The first column gives the peak cross sections calculated in PW approximation, including pion self-energies, and isobar medium effects (this is similar to the solid curve in Fig. 13). The second column gives the cross section with the total attenuation estimated from the eikonal calculation, including real pion absorption in the attenuation. In the third column, the spreading width has been included in the isobar self-energy, but real pion absorption was not included in the eikonal calculation. The overall distortion effects thus decrease the peak cross sections relative to the PW calculations by a factor 10–30. The reasonable agreement between the second and third columns shows consistency in the two methods for including the spreading width effect.[42] Similar reductions in the cross sections can be expected over the entire kinematic range for the experiment. Thus, from Table III these calculations predict peak cross sections of the order of 1–50 μb per steradian squared per MeV for this reaction.

IV. CONCLUSIONS AND FUTURE OUTLOOK

The results in the preceding section suggest that the coincidence cross sections for the reaction (p,p'π^+) should be measurable with present detectors and beam intensities. Preliminary results indicate that if the outgoing proton energy is fixed and the pion angle varied, the resulting angular distribution is sensitive primarily to nuclear transition densities. If the pion angle is fixed (near the peak of the cross section), then the shape of the proton energy spectrum is determined by the isobar propagator. For example, if one considers low values of the outgoing proton energy, the "projectile excitation" amplitude dominates the cross sections; for higher proton energies, the spectrum is dominated by amplitude "*D*." The separation between these two peaks increases with in-

cident proton energy.

Nuclear medium effects on the intermediate pion are found to be large, particularly for the "projectile excitation" term. In fact, if the pion self-energy is calculated without including the short-ranged repulsion in the particle-hole interaction, the PW calculations produce poles in the theoretical cross sections. Inclusion of short-ranged repulsion via a Migdal parameter with a reasonable strength renormalizes the self-energy; however, the net effect of the pion self-energy is still a considerable enhancement of the "projectile excitation" term, and a corresponding increase in the calculated cross sections. Medium effects on the isobar are found to be relatively small. There is considerable cancellation between the increase in the cross sections due to the combined dispersive and Pauli effects, and the decrease due to spreading-width effects.

The $(\omega$-$q)$ domain, in which the pion self-energy enhancements are largest, is the same region where "precursive" effects have been predicted in the past.[16,43–47] Many large effects predicted from such calculations have not been observed; thus there is considerable uncertainty regarding the magnitude of the pion self-energy in this region. It is therefore desirable to determine this quantity from experiment. The $(p,p'\pi^+)$ reaction, due to its strong sensitivity to the self-energy, may help to determine this quantity. Since different amplitudes from Fig. 1 are affected differently by the medium effects on the pion propagator, even the shape of the proton energy spectrum may provide a measure of the pion self-energy enhancement.

The present results have been obtained using the PW approximation. Effects of distortions were estimated from an eikonal approximation for the nuclear elastic scattering interactions of the protons and the pion. The predicted cross sections are reduced by at least an order of magnitude from the PW estimates, with the major reduction arising from the final-state pion-nucleus interaction. Care must be taken to avoid over-counting effects in the isobar propagator, and also in the pion-nucleus final-state interaction. In the present treatment, effects of final-state distortions have been applied only to the peak cross sections, where these ambiguities are less important than in other kinematic regions. Consistent results were obtained if the effects of true pion absorption were included either through the medium modification of the isobar, or in the pion-nucleus distortions.

The amplitudes for $(p,p'\pi^+)$ are proportional to spin-isospin and isospin nuclear transition densities and transition density matrices. With the simple wave functions used in this paper, we have not considered effects associated with (a) spin and isospin selectivity of reactions to particular nuclear states; (b) modification of the angular distributions due to more realistic bound nucleon orbitals; (c) out-of-plane measurements. It may be useful to make some qualitative remarks regarding this first point. To illustrate the effects of isospin selectivity, consider for example the reactions $(p,p'\pi^+)$, $(p,n\pi^+)$, and $(p,n\pi^-)$ on a closed-shell $T=0$ nucleus. For the reaction $(p,p'\pi^+)$ one trivially obtains the result that only $T=1$ final nuclear particle-hole states can be excited. For the $(p,n\pi^+)$ reaction, on the other hand, transitions to $T=0$ states are possible. But these transitions receive contributions only from the amplitudes C and D of Fig. 1. The "projectile-excitation" and "target-excitation" amplitudes of Figs. 1(a) and 1(b) do not contribute as the total spin of the neutron and pion for these diagrams is required to be $\frac{3}{2}$; consequently they contribute only to $T=1$ nuclear excitations. Furthermore, since in our model the transition density $\rho^{\sigma\tau}$ in amplitudes A and D represents an excitation mediated by an intermediate pion, such amplitudes permit only transitions to abnormal-parity nuclear states, viz., $(0^-,1^+,2^-,\ldots)$.

Finally, the present model does not contribute to the $(p,n\pi^-)$ reaction, which requires a change of two units in the nuclear charge. Such a change requires the participation of more than one target nucleon. The above selection rules can be of great utility in enhancing or suppressing the four amplitudes considered thus far. They can thus be used to study the reaction mechanism we have postulated.

An alternative approach might be to parametrize the $NN\rightarrow NN\pi$ amplitude, to extrapolate this to the kinematic region appropriate for these reactions, and fold it with the nuclear single-particle wave functions. This method is similar to that previously employed by Fearing,[48] and Sternheim and Silbar,[49] among others, for the (p,π) reaction. For the $(N,N'\pi)$ reaction, such an approach could be quite promising. First, it normalizes the results to the basic amplitude, pion production in two-nucleon interactions, for this reaction. The physical amplitudes for this process naturally incorporate the effects from resonant (isobar) and nonresonant intermediate states. Second, embedding the elementary amplitude in the nuclear medium is likely to give reasonable estimates for spin-dependent effects. Several groups[50] have noted the similarities between spin effects in (p,π) reactions and spin effects in the production of pions in two-nucleon interactions. Third, comparison of our results with those obtained by folding the elementary amplitude with nuclear wave functions would provide a benchmark for the importance of medium effects in this reaction.

In conclusion, our calculation has provided quantitative estimates of the size and shape of the spectra for this reaction, and gives encouraging predictions both for the size of the expected cross sections and the physics which can be extracted from such measurements. The $(N,N'\pi)$ reaction is potentially a powerful tool for investigating the dynamics of pions and isobars in nuclei, as it can investigate the nuclear response over a wide range of energy and momentum transfers. The spin-isospin selectivity of the reaction can be utilized to focus on individual amplitudes in the reaction mechanism. Once understood, this reaction could be exploited to test our knowledge of spin-isospin nuclear transition densities in the region of moderate to very large momentum transfer.

It is now essential to make more quantitative calculations in which the simplifying assumptions and approximations of this work are removed. Subsequent calculations should utilize proper distorted waves and realistic nuclear wave functions; useful comparisons can be made by embedding the "elementary" $NN\rightarrow NN\pi$ amplitude

in the nuclear medium. We are presently undertaking calculations which address these questions.

ACKNOWLEDGMENTS

Much of the work reported in this paper was carried out during two successive summers when one of the authors (B.K.J.) was visiting the Indiana University Nuclear Theory Center, and Cyclotron Facility. He gratefully acknowledges the financial support provided to him for these visits, and the warm hospitality of the members of both the Centers. The research was supported in part by the U.S. National Science Foundation under Contract No. NSF-PHY86-06364.

APPENDIX A: EVALUATION OF CROSS SECTIONS

The amplitudes for the (p,p'π^+) reaction proceeding via an intermediate Δ state give rise to four terms, shown diagrammatically in Figs. 1(a)–1(d). The first amplitude corresponds to emission of a virtual pion from a target nucleon, excitation of the incident proton of momentum $\mathbf{k}$ to a $\Delta(1232)$, with subsequent decay to a continuum proton and pion, with momenta $\mathbf{k}'$ and $\mathbf{k}_\pi$, respectively. This amplitude is referred to either as the "projectile excitation" term, or alternatively as "amplitude A" [referring to the diagram of Fig. 1(a)]. This amplitude has the form

$$T_A=\sqrt{2}\rho_{fi}(\mathbf{q}_A)\frac{f_\pi f_\Delta^2}{m_\pi^3}F(q_A)\times\frac{\langle f\,|\,\boldsymbol{\sigma}\cdot\mathbf{q}_A\,|\,i\rangle\langle k'\,|\,\mathbf{S}^\dagger\cdot\mathbf{k}_\pi\mathbf{S}\cdot\mathbf{q}_A\,|\,k\rangle}{D_\Delta(q_A^\Delta,\omega_A^\Delta)D_\pi(q_A,\omega_A)} \tag{A1}$$

where

$$\mathbf{q}_A=\mathbf{k}_\pi+\mathbf{k}'-\mathbf{k},\quad \omega_A=\epsilon_f-\epsilon_i\approx 0\ ,$$
$$\mathbf{q}_A^\Delta=\mathbf{k}_\pi+\mathbf{k}',\quad \omega_A^\Delta=E'+E_\pi\ . \tag{A2}$$

The second term corresponds to emission of a pion by the projectile proton, as shown in Fig. 1(b). This pion excites a target nucleon to a Δ, which then decays to the final continuum proton and pion. This amplitude is called either the "target excitation" term, or "amplitude B." This amplitude has the form

$$T_B=\sqrt{2}\frac{f_\pi f_\Delta^2}{m_\pi^3}\int\frac{d\mathbf{q}}{(2\pi)^3}\frac{F(q)\phi_f^\dagger(\mathbf{k}-\mathbf{q})\phi_i(\mathbf{k}'+\mathbf{k}_\pi-\mathbf{q})}{D_\Delta(q_B^\Delta,\omega_B^\Delta)D_\pi(q,\omega_B)}\times\langle f\,|\,\boldsymbol{\sigma}\cdot\mathbf{q}\,|\,k\rangle\langle k'\,|\,\mathbf{S}^\dagger\cdot\mathbf{k}_\pi\mathbf{S}\cdot\mathbf{q}\,|\,i\rangle\ , \tag{A3}$$

where

$$\omega_B=T_{\rm p}+\epsilon_f\approx T_{\rm p}\ ,$$
$$\mathbf{q}_B^\Delta=\mathbf{k}'+\mathbf{k}_\pi=\mathbf{q}_A^\Delta\ , \tag{A4}$$
$$\omega_B^\Delta=E'+E_\pi=\omega_A^\Delta\ .$$

The third amplitude, given in Fig. 1(c), referred to as "amplitude C," is obtained from "amplitude A" by exchanging the continuum and bound nucleon lines in the final state. It has the form

$$T_C=-\frac{\sqrt{2}}{3}\frac{f_\pi f_\Delta^2}{m_\pi^3}\int\frac{d\mathbf{q}}{(2\pi)^3}\frac{F(q)\phi_f^\dagger(\mathbf{k}-\mathbf{k}_\pi-\mathbf{q})\phi_i(\mathbf{k}'-\mathbf{q})}{D_\Delta(q_C^\Delta,\omega_C^\Delta)D_\pi(q,\omega_C)}\times\langle k'\,|\,\boldsymbol{\sigma}\cdot\mathbf{q}\,|\,i\rangle\langle f\,|\,\mathbf{S}^\dagger\cdot\mathbf{k}_\pi\mathbf{S}\cdot\mathbf{q}\,|\,k\rangle\ , \tag{A5}$$

where

$$\omega_C=-\epsilon_i-T_{\rm p'}\approx -T_{\rm p'}\ ,$$
$$\mathbf{q}_C^\Delta\approx\mathbf{k}_\pi\ , \tag{A6}$$
$$\omega_C^\Delta\approx E_\pi+M_{\rm p}\ .$$

The final amplitude is obtained by exchanging the bound and continuum nucleon lines in the final state of the "target excitation" amplitude. This term, shown in Fig. 1(d) and called "amplitude D," has the form

$$T_D=\frac{-\sqrt{2}}{3}\rho_{fi}(\mathbf{q}_A)\frac{f_\pi f_\Delta^2}{m_\pi^3}F(q_D)\times\frac{\langle k'\,|\,\boldsymbol{\sigma}\cdot\mathbf{q}_D\,|\,k\rangle\langle f\,|\,\mathbf{S}^\dagger\cdot\mathbf{k}_\pi\mathbf{S}\cdot\mathbf{q}_D\,|\,i\rangle}{D_\Delta(q_D^\Delta,\omega_D^\Delta)D_\pi(q_D,\omega_D)}\ , \tag{A7}$$

where

$$\mathbf{q}_D=\mathbf{k}'-\mathbf{k}\ ,$$
$$\omega_D=T_{\rm p'}-T_{\rm p}\ ,$$
$$\mathbf{q}_D^\Delta\approx\mathbf{k}_\pi\ , \tag{A8}$$
$$\omega_D^\Delta\approx E_\pi+M_{\rm p}\ .$$

In Eqs. (A1), (A3), (A5), and (A7), the form factor is taken to be of monopole form,

$$F(q)=\left[\frac{\Lambda^2-m_\pi^2}{\Lambda^2-\omega^2+\mathbf{q}^2}\right]^2\ , \tag{A9}$$

where the range is taken to be $\Lambda=1200$ MeV/c. The same cutoff is used for both NNπ and N$\Delta\pi$. In the latest Bonn NN potential,[18] the coupling constants are $\Lambda=1200$ MeV/c for the NNπ form factor, and $\Lambda=1300$ MeV/c for the ΔNπ form factor. The NNπ and N$\Delta\pi$ coupling constants are chosen to be

$$\frac{f_\pi^2}{4\pi}=0.08\ ,$$
$$\frac{f_\Delta^2}{4\pi}=0.37\ . \tag{A10}$$

The NNπ coupling constant is very well known from N-N scattering. The N$\Delta\pi$ coupling constant reproduces the experimental Δ decay width on resonance.[16] In Eqs. (A6) and (A8), the bound nucleon momentum has been neglected in the Δ propagator; with this approximation, the propagator is independent of the pion momentum q, and can be taken out of the integrals in Eqs. (A5) and

(A7).

For the single-particle transition densities and wave functions, simple Gaussian forms have been adopted,

$$\phi(p)=\left[\frac{4\pi}{p_0^2}\right]^{3/4}\exp(-p^2/2p_0^2)\ , \tag{A11}$$

$$\rho(p)=\exp(-p^2/4p_0^2)\ . \tag{A12}$$

The single-particle momentum scale p_0 has been fixed by requiring that it satisfy the relation $p_0^2=\frac{2}{3}\langle p^2\rangle=\frac{2}{5}k_F^2$, appropriate for quasifree electron scattering from a Fermi gas.

The pion and Δ propagators we take to have the form

$$D_\pi(\mathbf{q},\omega)=[\omega^2-\mathbf{q}^2-m_\pi^2-\Pi(\mathbf{q},\omega)+i\epsilon]^{-1}\ , \tag{A13}$$

where Π is the self-energy of the pion with momentum q and energy ω. The calculation of the self-energy Π is outlined in detail in Appendix B. Similarly, the Δ propagator is given by the relation

$$D_\Delta(\mathbf{q},\omega)=\left[\omega-\frac{q^2}{2m_\Delta}-M_\Delta-\mathcal{V}_\Delta(q,\omega)+i\Gamma/2+i\epsilon\right]^{-1}\ , \tag{A14}$$

where $\mathcal{V}$ represents the real part of the Δ-nucleus potential for a particle with energy ω and momentum q, Γ is the isobar width, and the isobar-nucleus interaction has been approximated with a local effective potential.[31]

The c.m. differential cross section is given in terms of the amplitudes as

$$\frac{d^3\sigma}{d\Omega' d\Omega_\pi dE'}=\frac{10^4}{2(2\pi)^5}\frac{k'k_\pi E'E}{k(1+E/E_A)}|T_{fi}|^2\ . \tag{A15}$$

In Eq. (A15), the units are μb/sr^2/MeV, and $|T_{fi}|^2$ is obtained by squaring the amplitudes of Eqs. (A1), (A3), (A5), and (A7), averaging over initial spins and summing over final spins. The cross sections are calculated for an unpolarized incident proton, neglecting the distortion of the incident and outgoing hadrons. The reaction is assumed to take place between the projectile proton and a single "active" proton in the nucleus, producing a continuum proton and a bound neutron. With the simple Gaussian wave functions of Eqs. (A11) and (A12), the PW cross sections in this model can be reduced to a sum of terms requiring no more than a single integral. These terms are listed in the following equations.

The square of the transition amplitude can be written as a sum of nine terms:

$$|T_{fi}|^2=|T_A|^2+|T_B|^2+|T_C|^2+|T_D|^2+T_{AB}+T_{AC}+T_{BD}+T_{BC}+T_{CD}\ . \tag{A16}$$

The interference term T_{AD} can be shown to vanish identically.

The first two amplitudes require no integration; they can be written as

$$|T_A|^2=cF(q_A)^2\exp\left[\frac{-q_A^2}{2p_0^2}\right]q_A^2\times\frac{[4(\mathbf{k}_\pi\cdot\mathbf{q}_A)^2+(\mathbf{k}_\pi\times\mathbf{q}_A)^2]}{|D_A^\Delta\cdot D_A^\pi|^2}\ , \tag{A17}$$

where the coefficient c is common to every term, defined as

$$c=2\left[\frac{f_\pi f_\Delta^2}{3m_\pi^3}\right]^2\ , \tag{A18}$$

$$|T_D|^2=cF(q_D)^2\exp\left[\frac{-q_A^2}{2p_0^2}\right]\times q_D^2\frac{[4(\mathbf{k}_\pi\cdot\mathbf{q}_D)^2+(\mathbf{k}_\pi\times\mathbf{q}_D)^2]}{9|D_D^\Delta\cdot D_D^\pi|^2}\ . \tag{A19}$$

The amplitude T_B can be evaluated most easily by defining the vector $\mathbf{R}$,

$$\mathbf{R}=\mathbf{k}+\mathbf{k}'+\mathbf{k}_\pi\ , \tag{A20}$$

and calculating angles of vectors relative to $\mathbf{R}$. For example, we define

$$\tilde{\theta}_\pi=\theta_\pi-\theta_R\ . \tag{A21}$$

An angle with a tilde represents the angle between that vector and the vector $\mathbf{R}$. With this convention,

$$|T_B|^2=c\,|a_B|^2[(1+3\cos^2\tilde{\theta}_\pi)|I_1|^2+(2+3\sin^2\tilde{\theta}_\pi)|I_2|^2]\ , \tag{A22}$$

where

$$a_B=\frac{4k_\pi}{\sqrt{\pi}D_\Delta(\omega_B^\Delta)p_0R}\exp\{-[k^2+(\mathbf{k}'+\mathbf{k}_\pi)^2]/2p_0^2\}\ , \tag{A23}$$

and

$$I_1=\int_0^\infty\frac{dq\,q^3\exp(-q^2/p_0^2)F(q)}{D_\pi(q,\omega_B)}\times[\sinh(u)-2\cosh(u)/u+2\sinh(u)/u^2]\ ,$$

$$I_2=\int_0^\infty\frac{dq\,q^3\exp(-q^2/p_0^2)F(q)}{D_\pi(q,\omega_B)}\times[\cosh(u)/u-\sinh(u)/u^2]\ , \tag{A24}$$

where

$$u=\frac{qR}{p_0^2}\ . \tag{A25}$$

$|T_C|^2$ is identical in form to the term $|T_B|^2$; it has the form

$$|T_C|^2 = c\,|a_C|^2[(1+3\cos^2\tilde{\theta}_{\pi'})|\tilde{I}_1|^2 + (2+3\sin^2\tilde{\theta}_{\pi'})|\tilde{I}_2|^2] . \quad \text{(A26)}$$

In Eq. (A26), $\tilde{I}_1$ and $\tilde{I}_2$ are obtained from I_1 and I_2 of Eq. (A24) by the substitutions

$$\omega_B \to \omega_C ,\quad \mathbf{R} \to \mathbf{R}' ,\quad \tilde{\theta}_\pi \to \tilde{\theta}_{\pi'} , \quad \text{(A27)}$$

where $\mathbf{R}'$ is defined by

$$\mathbf{R}' = \mathbf{k} + \mathbf{k}' - \mathbf{k}_\pi , \quad \text{(A28)}$$

and where

$$\tilde{\theta}_{\pi'} = \theta_\pi - \theta_{R'} . \quad \text{(A29)}$$

Any angle defined with both a tilde and a prime represents the angle between that vector and $\mathbf{R}'$. The overall coefficient a_C in Eq. (A26) is defined by

$$a_C = \frac{4k_\pi}{3\sqrt{\pi}p_0 R' D_\Delta(\omega_C^\Delta)} \exp\{-[k'^2 + (\mathbf{k}-\mathbf{k}_\pi)^2]/2p_0^2\} . \quad \text{(A30)}$$

The interference term T_{AB} can be defined as

$$T_{ab} = 2c\,\text{Real}[c_{AB}(u_{AB}I_1 + v_{AB}I_2)] , \quad \text{(A31)}$$

where

$$c_{AB} = \frac{4k_\pi^2 q_A^2}{\sqrt{\pi}p_0 R} \frac{\exp\{-[q_A^2/2 + k^2 + (\mathbf{k}'+\mathbf{k}_\pi)^2]/2p_0^2\}}{[D_\Delta^A D_\pi^A]^\dagger D_\Delta^B} , \quad \text{(A32)}$$

$$u_{AB} = -2\cos^2(\tilde{\theta}_A - \tilde{\theta}_\pi) - 2\cos^2(\tilde{\theta}_\pi) + 7\cos(\tilde{\theta}_A - \tilde{\theta}_\pi)\cos(\tilde{\theta}_A)\cos(\tilde{\theta}_\pi) + \cos^2(\tilde{\theta}_A) ,$$
$$v_{AB} = -3\cos^2(\tilde{\theta}_A - \tilde{\theta}_\pi) - 2\sin^2(\tilde{\theta}_\pi) + 7\cos(\tilde{\theta}_A - \tilde{\theta}_\pi)\sin(\tilde{\theta}_A)\sin(\tilde{\theta}_\pi) - \cos^2(\tilde{\theta}_A) , \quad \text{(A33)}$$

and I_1 and I_2 are given in Eq. (A24).

The interference term T_{CD} is given by

$$T_{CD} = 2c\ \text{Re}[c_{CD}(u_{CD}\tilde{I}_1 + v_{CD}\tilde{I}_2)] . \quad \text{(A34)}$$

In this equation, $\tilde{I}_1$ and $\tilde{I}_2$ are defined from Eqs. (A24) and Eqs. (A27)–(A29). The coefficients u_{CD} and v_{CD} are obtained from u_{AB} and v_{AB} of Eq. (A33) by the replacements

$$\tilde{\theta}_A \to \tilde{\theta}_{A'} ,\quad \tilde{\theta}_\pi \to \tilde{\theta}_{\pi'} . \quad \text{(A35)}$$

Finally, the coefficient c_{CD} is given by

$$c_{CD} = \frac{4k_\pi^2 q_D^2}{9\sqrt{\pi}p_0 R'} \frac{\exp\{-[q_D^2/2 + k^2 + (\mathbf{k}'+\mathbf{k}_\pi)^2]/2p_0^2\}}{[D_\Delta^D D_\pi^D]^\dagger D_\Delta^C} . \quad \text{(A36)}$$

The interference term T_{AC} is given by

$$T_{AC} = 2c\,\text{Real}[c_{AC}(v_{AC}\tilde{I}_1 + v_{AC}\tilde{I}_2)] , \quad \text{(A37)}$$

where $\tilde{I}_1$ and $\tilde{I}_2$ are given by Eq. (A26), and

$$c_{AC} = -\frac{4k_\pi^2 q_A^2}{3\sqrt{\pi}p_0 R'} \times \frac{\exp\{-[q_A^2/2 + k'^2 + (\mathbf{k}-\mathbf{k}_\pi)^2]/2p_0^2\}}{[D_\Delta^A D_\pi^A]^\dagger D_\Delta^C} . \quad \text{(A38)}$$

The coefficients u_{AC} and v_{AC} are defined by

$$u_{AC} = 2\cos^2(\tilde{\theta}_{A'} - \tilde{\theta}_{\pi'}) + 2\cos^2(\tilde{\theta}_{\pi'}) - \sin(\tilde{\theta}_{A'} - \tilde{\theta}_{\pi'})\cos(\tilde{\theta}_{A'})\sin(\tilde{\theta}_{\pi'}) ,$$
$$v_{AC} = 4\cos^2(\tilde{\theta}_{A'} - \tilde{\theta}_{\pi'}) + 2\sin^2(\tilde{\theta}_{\pi'}) + \sin(\tilde{\theta}_{A'} - \theta_{\pi'})\cos(\tilde{\theta}_{A'})\sin(\tilde{\theta}_{\pi'}) . \quad \text{(A39)}$$

The interference term T_{BD} is given by the equation

$$T_{BD} = 2c\ \text{Re}[c_{BD}(u_{BD}I_1 + v_{BD}I_2)] , \quad \text{(A40)}$$

where

$$c_{BD} = -\frac{4k_\pi^2 q_D^2}{3\sqrt{\pi}p_0 R} \frac{\exp\{-[q_A^2/2 + k^2 + (\mathbf{k}'+\mathbf{k}_\pi)^2]/2p_0^2\}}{[D_\Delta^D D_\pi^D]^\dagger D_\Delta^B} , \quad \text{(A41)}$$

and where u_{BD} and v_{BD} are obtained from u_{AC} and v_{AC}, respectively, of Eq. (A39), by replacing

$$\theta_A \to \theta_D \quad \text{(A42)}$$

in all angles. In Eq. (A42), θ_A and θ_D are the polar angles of the vectors $\mathbf{q}_A$ and $\mathbf{q}_D$, defined in Eqs. (A2) and (A8), respectively. Remember that $\tilde{\theta}_{A'}$ in Eq. (A39) is defined by

$$\tilde{\theta}_{A'} = \theta_A - \theta_{R'} . \quad \text{(A43)}$$

The final interference term is given by

$$T_{BC} = 2c\,\text{Real}\{a_B a_c^\dagger[2\cos\tilde{\theta}_\pi\cos\tilde{\theta}'_\pi I_2\tilde{I}_2^\dagger + \sin\tilde{\theta}_\pi\sin\tilde{\theta}'_\pi(I_2\tilde{I}_1^\dagger + I_1\tilde{I}_2^\dagger)]\} \quad \text{(A44)}$$

where the angles $\tilde{\theta}_\pi$ and $\tilde{\theta}_{\pi'}$ are defined in Eqs. (A21) and (A29), respectively.

APPENDIX B: CALCULATION OF PION SELF-ENERGY CONTRIBUTIONS

For the pion self-energy contributions calculated in Sec. III B, we first calculate the contributions from particle-hole states. These particle-hole amplitudes are shown schematically in Fig. 7(a). The full meson propagator is given by

$$G(q,\omega)=\frac{G_0(q,\omega)}{1-G_0(q,\omega)\Pi^0(q,\omega)}\ , \tag{B1}$$

where the free propagator is given as

$$G_0(q,\omega)=[\omega^2-q^2-m^2+i\eta]^{-1}\ . \tag{B2}$$

The self-energy Π^0 due to these terms is given by

$$\Pi^0(q,\omega)=4\left[\frac{qf_\pi(q)}{m_\pi}\right]^2\int\frac{d\mathbf{k}}{(2\pi)^3}\left[\frac{n(\mathbf{k})(1-n(\mathbf{k}+\mathbf{q}))}{\omega-\epsilon(\mathbf{k}+\mathbf{q})+\epsilon(\mathbf{k})+i\eta}+\frac{n(\mathbf{k})(1-n(\mathbf{k}+\mathbf{q}))}{-\omega-\epsilon(\mathbf{k}+\mathbf{q})+\epsilon(\mathbf{k})+i\eta}\right]\ . \tag{B3}$$

Inserting the self-energy from Eq. (B3) into the equation for the propagator, Eq. (B1), sums the ring diagrams for the self-energy contributions, as is well known.[24] The nuclear density is approximated by a Fermi gas, for which the occupation probability takes the form $n(k)=\theta(k_F-k)$. The particle (hole) kinetic energy is given by $\epsilon(k)=k^2/2M^*+M_N$, where the effective mass M^* is taken as $M^*=0.7M_N$. The following dimensionless quantities are defined:

$$\begin{aligned}&\tilde{q}=q/k_F\ ,\\ &\nu=\frac{M^*\omega}{k_F^2}\ ,\\ &q_+=\tilde{q}/2+\nu/\tilde{q}\ ,\\ &q_-=\tilde{q}/2-\nu/\tilde{q}\ .\end{aligned} \tag{B4}$$

In terms of these quantities, the real part of the self-energy takes the form

$$\mathrm{Re}\Pi^0(q,\omega)=-4\left[\frac{qf_\pi(q)}{m_\pi}\right]^2\frac{M^*k_F}{(2\pi)^2}\left[1+\frac{1}{2\tilde{q}}(1-q_-^2)\ln\left|\frac{1+q_-}{1-q_-}\right|+\frac{1}{2\tilde{q}}(1-q_+^2)\ln\left|\frac{1+q_+}{1-q_+}\right|\right]\ . \tag{B5}$$

The imaginary part of the self-energy due to particle-hole terms has the form

$$\begin{aligned}\mathrm{Im}\Pi^0(q,\omega)&=-\left[\frac{qf_\pi(q)}{m_\pi}\right]^2\frac{M^*k_F}{2\pi\tilde{q}}[1-q_-^2],\quad \tilde{q}>2,\quad \tilde{q}^2/2-\tilde{q}\le\nu\le\tilde{q}^2/2+\tilde{q}\\ &=-\left[\frac{qf_\pi(q)}{m_\pi}\right]^2\frac{M^*k_F}{2\pi\tilde{q}}[1-q_-^2],\quad \tilde{q}<2,\quad \tilde{q}-\tilde{q}^2/2\le\nu\le\tilde{q}^2/2+\tilde{q}\\ &=-\left[\frac{qf_\pi(q)}{m_\pi}\right]^2\frac{M^*k_F\nu}{\pi\tilde{q}},\quad \tilde{q}<2,\quad 0\le\nu\le\tilde{q}-\tilde{q}^2/2\ ,\end{aligned} \tag{B6}$$

and $\mathrm{Im}\Pi^0(q,\omega)$ is 0 for all other values of q and ω.

The Δ-hole contribution to the pion self-energy is given by the contributions of Fig. 7(b), and has been calculated in Ref. 25. It has the form

$$\Pi^0_\Delta(q,\omega)=\left[\frac{4qf_\Delta(q)}{3m_\pi}\right]^2\int\frac{d\mathbf{k}}{(2\pi)^3}\theta(k_F-k)\left[\frac{1}{\omega-\epsilon_\Delta(\mathbf{k}+\mathbf{q})+\epsilon(\mathbf{k})+i\eta}+\frac{1}{-\omega-\epsilon_\Delta(\mathbf{k}+\mathbf{q})+\epsilon(\mathbf{k})+i\eta}\right]\ . \tag{B7}$$

In Eq. (B7), the Δ total energy for a particle of momentum p, arising from a pion of energy ω, is given by

$$\epsilon_\Delta(p)=p^2/2M_\Delta+M_\Delta-\frac{i\Gamma(\omega)}{2}\ . \tag{B8}$$

In Eq. (B8), Γ represents the Δ width in the medium. This represents the contributions of these diagrams to absorption from a propagating meson. Clearly, this will depend on the energy ω of the meson producing the Δ-hole pair. The following prescription has been chosen for Γ. For the direct graphs, Γ was taken as the free width $\Gamma_0=116$ MeV if the meson energy was greater than the $\Delta-N$ mass difference; otherwise, Γ was taken as a fraction of the free width. For the crossed graphs of Fig. 7(b), the width was set to zero. Specifically

$$\begin{aligned}\Gamma(\omega)&=\left[\frac{\omega-m_\pi}{\delta M-m_\pi}\right]^{3/2}\Gamma_0,\quad \omega\le\delta M\equiv M_\Delta-M_N\ ,\\ &=\Gamma_0,\quad \omega>\delta M\ .\end{aligned} \tag{B9}$$

Performing the integrations in Eq. (B7) gives

$$\Pi^0_\Delta(q,\omega)=-\left[\frac{4qf_\Delta(q)}{3m_\pi}\right]^2\frac{M_\Delta k_F}{(2\pi)^2\tilde{q}}\left[\tilde{q}+\alpha_- -\alpha_+ +\tfrac{1}{2}(1-q_+^2)\ln\left[\frac{1+q_+}{-1+q_+}\right]+\tfrac{1}{2}(1-q_-^2)\ln\left[\frac{1+q_-}{-1+q_-}\right]\right]. \quad \text{(B10)}$$

The quantities in Eq. (B10) are defined as

$$\begin{aligned}\tilde{q}&=q/k_F\ ,\\ \alpha_\pm&=\frac{M_\Delta}{qk_F}\left[\omega\mp\delta M+\frac{i\Gamma(\pm\omega)}{2}\right],\\ q_+&=\tilde{q}/2-\alpha_+\ ,\\ q_-&=\tilde{q}/2+\alpha_-\ .\end{aligned} \quad \text{(B11)}$$

When all the arguments in Eq. (B10) are real, the absolute values of the arguments of the logarithms are used.

In the preceding equations, the short-ranged repulsion between particle-hole and isobar-hole pairs has not been included. As a result, the pion self-energy calculated from Eqs. (B3) and (B7) is so large that it produces zeroes in the full Green function of Eq. (B1) and poles in the resulting cross sections (see Fig. 8, and the discussion in Sec. III B). As is well known,[16,19] the poles result from the improper treatment of the short-range behavior, and a short-ranged repulsion must be included in order to remove the spurious poles from the full Green function. This short-ranged repulsion is parametrized through the Migdal parameters, which are supposed to mock up the complicated density-dependent effective interaction between particles and holes in the nuclear medium. The additional short-range piece has the form

$$\begin{aligned}W_{\text{p.h.}}=&\frac{f_\pi^2}{m_\pi^2}g'\boldsymbol{\sigma}_1\cdot\boldsymbol{\sigma}_2\boldsymbol{\tau}_1\cdot\boldsymbol{\tau}_2+\frac{f_\Delta^2}{m_\pi^2}g'\mathbf{S}_1^\dagger\cdot\mathbf{S}_2\mathbf{T}_1^\dagger\cdot\mathbf{T}_2\\&+\frac{f_\pi f_\Delta}{m_\pi^2}g'_{N\Delta}[\mathbf{S}_1\cdot\boldsymbol{\sigma}_2\mathbf{T}_1\cdot\boldsymbol{\tau}_2+\text{H.c.}]\ .\end{aligned} \quad \text{(B12)}$$

We sum all rings with short-ranged correlations in intermediate states, as shown in Fig. 7(c). The resulting renormalization of the self-energies is well known. If the self-energies are defined in terms of the "susceptibilities" as

$$\begin{aligned}\Pi_N&\equiv-q^2\chi_N\ ,\\ \Pi_\Delta&\equiv-q^2\chi_\Delta\ ,\end{aligned} \quad \text{(B13)}$$

then the susceptibilities get renormalized to

$$\chi_N\rightarrow\frac{1+\chi_\Delta(g'_{N\Delta}-g')}{(1+g'\chi_\Delta)(1+g'\chi_N)-(g'_{N\Delta})^2\chi_N\chi_\Delta}\chi_N(q,\omega)\ , \quad \text{(B14)}$$

$$\chi_\Delta\rightarrow\frac{1+\chi_N(g'_{N\Delta}-g')}{(1+g'\chi_\Delta)(1+g'\chi_N)-(g'_{N\Delta})^2\chi_N\chi_\Delta}\chi_\Delta(q,\omega)\ .$$

The calculations in this paper were done using $g'_{N\Delta}=g'$, in which case one obtains the renormalizations

$$\begin{aligned}\chi_N(q,\omega)&\rightarrow\frac{\chi_N(q,\omega)}{1+g'(\chi_N+\chi_\Delta)}\ ,\\ \chi_\Delta(q,\omega)&\rightarrow\frac{\chi_\Delta(q,\omega)}{1+g'(\chi_N+\chi_\Delta)}\ .\end{aligned} \quad \text{(B15)}$$

APPENDIX C: RELATIVISTIC CALCULATION OF PION SELF-ENERGY

In Appendix B, a nonrelativistic calculation of the pion self-energies, derived from NR NNπ and ΔNπ vertices and NR nucleon propagators, was outlined. One could also attempt to calculate the self-energy effects from relativistic propagators and Dirac spinors for the nucleons and isobar. In this procedure, a relativistic expression for the self-energy is derived; at some stage, the baryon kinetic energies are replaced by nonrelativistic values, since for the energies considered here the nucleon and isobar motion is well described by a low-order expansion in p/M. The resulting integrals are carried out using a relativistic Fermi gas model for the nuclear momentum distribution.

Such a calculation has been carried out by Dmitriev and Suzuki;[29] in this appendix, their derivations are repeated, and relativistic self-energy results compared with the NR results discussed earlier in this paper. In the formalism of Dmitriev and Suzuki, the self-energy is obtained by taking traces of Dirac matrices relevant to the particle-hole propagation of positive-energy intermediate states. They use pseudovector coupling for the NNπ vertex; their expression for the particle-hole self-energy, analogous to Eq. (B3), is

$$\begin{aligned}\Pi^0_R(q,\omega)=2\left[\frac{f_\pi}{m_\pi}\right]^2\int\frac{d^4p}{(2\pi)^3}\text{Tr}\Bigg[&\not{q}\gamma^5\frac{\not{p}+\not{q}+M}{2E_{p+q}}\not{q}\gamma^5\frac{\not{p}+M}{p_0^2-E_p^2+i\eta}n(p+q)\delta(p_0+\omega-E_{p+q})\\&+\not{q}\gamma^5\frac{\not{p}+\not{q}+M}{(p_0+\omega)^2-E_{p+q}^2+i\eta}\not{q}\gamma^5\frac{\not{p}+M}{2E_p}n(p)\delta(p_0-E_p)\\&+i\pi\frac{n(p)n(p+q)}{2E_pE_{p+q}}\delta(p_0-E_p)\delta(p_0+\omega-E_{p+q})\not{q}\gamma^5(\not{p}+\not{q}+M)\not{q}\gamma^5(\not{p}+M)\Bigg]\ . \quad \text{(C1)}\end{aligned}$$

Taking the trace in Eq. (C1), and using the fact that the nucleon motion is nonrelativistic (and hence $E_p \approx M + p^2/2M$) gives

$$\Pi_R^0(q,\omega) = -4\left[\frac{f_\pi}{m_\pi}\right]^2 t \int \frac{d^3p}{(2\pi)^3} n(p) \left[\frac{1}{t/2M + \mathbf{p}\cdot\mathbf{q}/M - \omega} + \frac{1}{t/2M - \mathbf{p}\cdot\mathbf{q}/M + \omega} + 2i\pi n(p+q)\delta(\omega - \mathbf{p}\cdot\mathbf{q}/M - q^2/2M) \right] . \tag{C2}$$

Performing the integral in Eq. (C2) with a Fermi gas nuclear momentum distribution gives

$$\mathrm{Re}\Pi_R^0(q,\omega) = -\frac{f_\pi(q)^2}{m_\pi^2}\frac{M^* k_F t}{(2\pi)^2}\left\{1 + \frac{1}{2\tilde{q}}[1-(q_-^R)^2]\ln\left|\frac{1+q_-^R}{1-q_-^R}\right| + \frac{1}{2\tilde{q}}[1-(q_+^R)^2]\ln\left|\frac{1+q_+^R}{1-q_+^R}\right|\right\} , \tag{C3}$$

$$\mathrm{Im}\Pi_R^0(q,\omega) = \frac{-t}{q^2}\mathrm{Im}\Pi^0(q,\omega) . \tag{C4}$$

The imaginary part of the relativistic and nonrelativistic particle-hole self-energies are proportional, as seen in Eq. (C4); the real parts have the same form, as seen by comparing Eq. (C3) with Eq. (B5). In the relativistic equation a new set of dimensionless quantities are defined by

$$q_+^R \equiv -\frac{\tilde{t}}{2\tilde{q}} + \frac{\nu}{\tilde{q}} ,$$

$$q_-^R \equiv -\frac{\tilde{t}}{2\tilde{q}} - \frac{\nu}{\tilde{q}} , \tag{C5}$$

where

$$\tilde{t} \equiv \frac{\omega^2 - |\mathbf{q}|^2}{k_F^2} . \tag{C6}$$

Thus, the relativistic and nonrelativistic particle-hole contributions to the pion self-energy differ only in the replacement of $-|\mathbf{q}|^2$ by $t = \omega^2 - |\mathbf{q}|^2$ in certain places. From Eq. (C3), the self-energy contribution goes to zero when $t=0$, in agreement with requirements of chiral symmetry and PCAC. Note that the most important contribution to the cross sections comes from "amplitude A" (see the discussion in Sec. III B). In this amplitude, $\omega \approx 0$; for this special case, the relativistic and nonrelativistic particle-hole self-energies are identical.

The relativistic Δ-hole contribution to the self-energy can be written as

$$\Pi_R^\Delta = \tfrac{4}{3}\left[\frac{f_\Delta}{m_\pi}\right]^2 \int \frac{d^4p}{(2\pi)^3}\mathrm{Trace}\left[\frac{2M_\Delta q^\mu q^\nu \Lambda_{\mu\nu}(p+q)}{(p_0+\omega)^2 - E_\Delta^2(p+q) + i\eta}\frac{\not{p}+M}{2E_p} n(p)\delta(p_0 - E_p) + q \leftrightarrow -q\right] , \tag{C7}$$

where $\Lambda_{\mu\nu}(p)$ is the relativistic spin-$\frac{3}{2}$ projection operator

$$\Lambda_{\mu\nu}(p) = -\frac{\not{p}+M_\Delta}{2M_\Delta}\left[g_{\mu\nu} - \tfrac{1}{3}\gamma_\mu\gamma_\nu - \frac{2p_\mu p_\nu}{3M_\Delta^2} + \frac{p_\mu\gamma_\nu - p_\nu\gamma_\mu}{3M_\Delta}\right] . \tag{C8}$$

Dmitriev and Suzuki evaluate this expression in the nonrelativistic limit, as $(p\cdot q)^2 - M^2 t \approx M^2 |\mathbf{q}|^2$; in this case,

$$\Pi_R^\Delta(q,\omega) = \Pi_{NP}^\Delta(q,\omega) + \left[\frac{(M+M_\Delta)^2 - t}{4M_\Delta^2}\right]\Pi_P^\Delta(q,\omega) , \tag{C9}$$

where the "nonpole" contribution to the Δ-hole amplitude is

$$\Pi_{NP}^\Delta(q,\omega) \equiv \left[\frac{4f_\Delta}{3m_\pi}\right]^2\left[\frac{M}{M_\Delta^2}\bar{n}q^2 + \frac{M+M_\Delta}{2M_\Delta^2}\bar{n}t\right] , \tag{C10}$$

and the "pole" contribution has the form

$$\Pi_P^\Delta(q,\omega) \equiv -\left[\frac{4qf_\Delta}{3m_\pi}\right]^2 \frac{M_\Delta k_F}{(2\pi)^2\tilde{q}}\left[-\frac{\tilde{t}}{\tilde{q}} - \alpha_+ + \alpha_- + \tfrac{1}{2}[1-(\tilde{q}_+)^2]\ln\left[\frac{1+\tilde{q}_+}{-1+\tilde{q}_+}\right] + \tfrac{1}{2}[1-(\tilde{q}_-)^2]\ln\left[\frac{1+\tilde{q}_-}{-1+\tilde{q}_-}\right]\right] . \tag{C11}$$

In Eq. (C10), $\bar{n}$ represents some averaged nuclear density. This has been chosen as $\bar{n}=0.11$ fm^{-3}, in agreement with the choice for the nuclear Fermi momentum, as discussed in Sec. III B. In Eq. (C11), all terms have the same meaning as in Eq. (B10), with the quantities $\tilde{q}_+$ and $\tilde{q}_-$ defined by

$$\tilde{q}_+ \equiv -\frac{\tilde{t}}{2\tilde{q}} - \alpha_+ ,$$
$$\tilde{q}_- \equiv -\frac{\tilde{t}}{2\tilde{q}} + \alpha_- . \qquad \text{(C12)}$$

In Fig. 14, the cross sections with relativistic pion self-energies are compared with the results obtained using the nonrelativistic formalism of Appendix B. The results are calculated for incident energy 450 MeV and Migdal parameter $g'=0.7$. The solid curve shows the results with the nonrelativistic self-energy; the dashed curve gives the results for the relativistic self-energy. The relativistic results are somewhat larger than the nonrelativistic results, although the two methods never disagree by more than a factor of two. The major difference between the two results is in the isobar-hole self-energy, due to the additional terms which arise because of the difference between the NR and relativistic isobar propagator. The difference between the two calculations of the self-energy gives one measure of the uncertainty in this quantity.

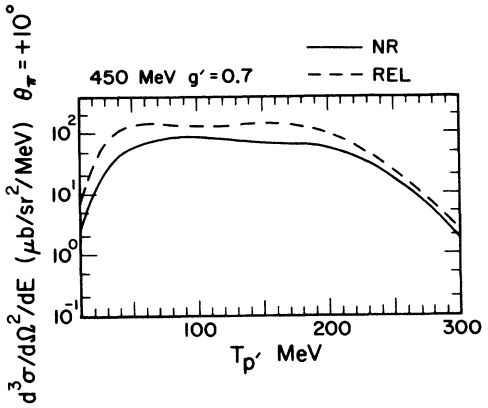

FIG. 14. Comparison of relativistic and nonrelativistic calculations of pion self-energy. Incident proton energy 450 MeV and pion angle + 10° vs outgoing proton energy. Migdal parameter $g'=0.7$. Solid curve, nonrelativistic self-energy; dashed curve, relativistic self-energy, calculated using the approximations of Dmitriev and Suzuki, Ref. 29.

[1]For a comprehensive set of references to the (p,π) problem up to 1981, see the *Proceedings of the Conference on Pion Production and Absorption in Nuclei,* AIP Conference Proceedings No. 79, edited by R. D. Bent (AIP, New York, 1982); see also W. W. Jacobs, in *Nuclear Structure at High Spin, Excitation and Momentum Transfer,* AIP Conference Proceedings No. 142, edited by H. Nann (AIP, New York, 1986).

[2]F. Soga *et al.*, Phys. Rev. C **22**, 1348 (1980); F. Soga *et al.*, *ibid.* **24**, 570 (1981); T. P. Sjoreen *et al.*, *ibid.* **24**, 1135 (1981); J. J. Kehayias *et al.*, *ibid.* **33**, 725 (1986); Z-J. Cao *et al.*, *ibid.* **35**, 825 (1987).

[3]W. W. Jacobs *et al.*, Phys. Rev. Lett. **49**, 855 (1982); S. E. Vigdor *et al.*, *ibid.* **49**, 1314 (1982); S. E. Vigdor *et al.*, Nucl. Phys. **A396**, 61c (1982); Z-J. Cao, R. D. Bent, H. A. Nann, and T. E. Ward, Phys. Rev. C **35**, 625 (1987); T. G. Throwe *et al.*, *ibid.* **35**, 1083 (1987); E. Korkmaz *et al.*, Phys. Rev. Lett. **58**, 104 (1987).

[4]D. F. Measday and G. A. Miller, Ann. Rev. Nucl. Part. Sci. **29**, 121 (1979); B. Hoistad, Adv. Nucl. Phys. **11**, 135 (1979).

[5]M. J. Iqbal and G. E. Walker, Phys. Rev. C **32**, 556 (1985).

[6]G. E. Walker, Comments Nucl. Part. Phys. **A11**, 169 (1983).

[7]P. W. F. Alons, R. D. Bent, J. S. Conte and M. Dillig, Indiana University Cyclotron Facility Report No. 390, 1987.

[8]E. D. Cooper and H. S. Sherif, Phys. Rev. C **25**, 3024 (1982); **25**, 732 (1984).

[9]Indiana University Cyclotron Facility Scientific and Technical Report, 1986.

[10]F. Shimizu, Y. Kubota, H. Koiso, F. Sai, S. Sakamoto, and S. S. Yamamoto, Nucl. Phys. **A386**, 571 (1982).

[11]F. Shimizu, H. Koiso, Y. Kubota, F. Sai, S. Sakamoto, and S. S. Yamamoto, Nucl. Phys. **A389**, 445 (1982).

[12]H. S. Sherif, S. W. Leung, A. W. Thomas, and G. Brookfield, Phys. Lett. **83B**, 293 (1979).

[13]J. M. Greben and R. M. Woloshyn, Nucl. Phys. **A333**, 399 (1980).

[14]E. D. Cooper, K. H. Hicks, and B. K. Jennings, Nucl. Phys. **A470**, 523 (1987).

[15]M. Hirata, F. Lenz, and K. Yazaki, Ann. Phys. (N.Y.) **108**, 116 (1977); M. Hirata, J. H. Koch, F. Lenz, and E. J. Moniz, *ibid.* **120**, 205 (1979); Y. Horikawa, M. Thies, and F. Lenz, Nucl. Phys. **A345**, 386 (1980); F. Lenz, E. J. Moniz, and K. Yazaki, Ann. Phys. (N.Y.) **129**, 84 (1980).

[16]E. Oset, H. Toki, and W. Weise, Phys. Rep. **83**, 282 (1982).

[17]A. B. Migdal, Rev. Mod. Phys. **50**, 107 (1978).

[18]R. Machleidt, K. Holinde, and Ch. Elster, Phys. Rep. **149**, 1 (1987).

[19]G. E. Brown and W. Weise, Phys. Rep. **22**, 279 (1975).

[20]Estimates of the relative size of these terms have been made in Refs. 5, 21, and 22. Such estimates are energy dependent, so these numbers should be used with some caution. An estimate of the energy dependence of the direct and crossed terms has been made in Ref. 23; for energies 350 and 450 MeV, the crossed terms should contribute only a few percent of the direct terms; at 800 MeV, the direct and crossed terms are likely to be of roughly equal size, before applying the isospin factors.

[21]B. D. Keister and L. S. Kisslinger, Nucl. Phys. **A412**, 301 (1984).

[22]B. K. Jain and S. C. Phatak, private communication.

[23]M. J. Iqbal, Ph.D. thesis, Indiana University, 1982 (unpublished).

[24]A. Fetter and J. D. Walecka, *Quantum Theory of Many-Particle Systems* (McGraw-Hill, New York, 1971).

[25]E. Oset and A. Palanques-Mestre, Nucl. Phys. **A359**, 289 (1981).
[26]G. E. Brown and W. Weise, Phys. Rep. **27**, 1 (1976).
[27]A. Arima *et al.*, Phys. Lett. **122B**, 126 (1983).
[28]B. K. Jain, Phys. Rev. C **29**, 1396 (1984).
[29]V. F. Dmitriev and T. Suzuki, Nucl. Phys. **A438**, 697 (1985).
[30]A. B. Santra and B. K. Jain, J. Phys. G **13**, 745 (1987).
[31]R. A. Freedman, G. A. Miller, and E. M. Henley, Nucl. Phys. **A389**, 457 (1982).
[32]The choice of a 35-MeV attractive real potential is a reasonable choice for incident proton energies around 400 MeV. This can be verified from isobar-hole calculations such as are described in Ref. 15, or from (p,π) calculations such as Ref. 5. However, for an 800 MeV proton incident energy, the size of the isobar-nucleus interaction is quite uncertain. Since this energy is quite a long distance from the isobar resonance, the numerical results depend only very weakly on the choice for the real part of the isobar-nucleus effective potential at 800 MeV energy.
[33]K. Stricker, H. McManus, and J. A. Carr, Phys. Rev. C **19**, 929 (1979).
[34]T. E. O. Ericson and J. Hüfner, Phys. Lett. **33B**, 601 (1970).
[35]M. Hirata, Phys. Rev. Lett. **40**, 704 (1978).
[36]M. Hirata, K. Masutani, A. Matsuyama, and K. Yazaki, Phys. Lett. **128B**, 15 (1983); K. Sakamoto, M. Hirata, A. Matsuyama, and K. Yazaki, Phys. Rev. C **31**, 1987 (1985).
[37]E. D. Cooper and A. Matsuyama, Nucl. Phys. **A460**, 699 (1986).
[38]As has been mentioned, the extent to which the resonant pion-nucleon amplitudes are double counted (in the isobar self-energy or in the final-state interaction), varies greatly from one amplitude to another. In this paper, the final-state effects are estimated only for certain kinematic values where only a single amplitude dominates the cross sections. The double-counting problem remains to be dealt with in a full distorted-wave calculation of this reaction.
[39]P. C. Tandy, E. F. Redish, and D. Bollè, Phys. Rev. C **16**, 1924 (1977).
[40]H. O. Meyer *et al.*, Phys. Rev. C **24**, 1782 (1981); A. Nadasen, Indiana University Cyclotron Facility Report No. 77-5 (unpublished).
[41]D. V. Bugg *et al.*, Phys. Rev. **146**, 980 (1966); S. Barshay, C. B. Dover, and J. P. Vary, Phys. Rev. C **11**, 360 (1975); K. Chen *et al.*, Phys. Rev. **166**, 949 (1968); R. H. Bassel and C. Wilkin, Phys. Rev. **174**, 1179 (1968).
[42]The cross sections are in substantial agreement, whether the real pion absorption is accounted for in the propagation of the isobar, or whether it is calculated as part of the final-state pion absorption. Nevertheless, both methods undercount the effects of absorption, since some of the real absorption should be included in both the isobar and the final-state pion.
[43]See Vol. III of *Mesons in Nuclei,* edited by M. Rho and D. H. Wilkinson (North-Holland, Amsterdam, 1979), particularly articles by A. B. Migdal, S.-O. Bäckman and W. Weise, G. Baym and D. K. Campbell, and R. F. Sawyer.
[44]M. Ericson and J. Delorme, Phys. Lett. **76B**, 241 (1978); M. Ericson, Nucl. Phys. **A335**, 309 (1980); J. Delorme, M. Ericson, A. Figureau, and N. Giraud, Phys. Lett. **89B**, 327 (1980); J. Delorme, A. Figureau, and P. Guichon, *ibid.* **99B**, 187 (1981).
[45]E. Oset and W. Weise, Phys. Lett. **77B**, 159 (1978); Nucl. Phys. **A319**, 477 (1979); **A329**, 365 (1979).
[46]H. Toki and W. Weise, Phys. Rev. Lett. **42**, 1034 (1979); Phys. Lett. **92B**, 265 (1980); Z. Phys. **A292**, 389 (1979).
[47]W. M. Alberico, M. Ericson, and A. Molinari, Phys. Lett. **92B**, 153 (1980).
[48]H. W. Fearing, Phys. Rev. C **16**, 313 (1977); **11**, 1210 (1975); **11**, 1493 (1975); in *Progress in Particle and Nuclear Physics,* edited by D. Wilkinson (Pergamon, Oxford, 1981), Vol. 7, p. 113.
[49]R. R. Silbar and M. M. Sternheim, Phys. Rev. C **8**, 492 (1973); M. M. Sternheim and R. R. Silbar, Phys. Rev. D **6**, 3117 (1972).
[50]For example, see the papers in Ref. 3 and references quoted in these papers.